# ADAPTING SOLID OXIDE FUEL CELLS TO OPERATE ON LANDFILL GAS. METHANE PASSIVATION OF Ni ANODE

**By**

**MOSES OHAKUMHE DOGHO**

**Submitted in Partial Fulfillment of the Requirements**

**for the Degree of**

**Master of Science**

**in the**

**Chemistry**

**Program**

**YOUNGSTOWN STATE UNIVERSITY**

**May 2023**

**ADAPTING SOLID OXIDE FUEL CELLS TO OPERATE ON LANDFILL GAS. METHANE PASSIVATION OF Ni ANODE**

I hereby grant permission to the public to access and use of this thesis. I acknowledge that it will be accessible through the OhioLINK ETD Center and the Maag Library Circulation Desk. Additionally, I authorize the university or any other individuals to reproduce copies of this thesis for scholarly research purposes.

Signature:

…….. …….

Moses Dogho, Student Date

Approvals:

…….. …….

Dr. Clovis A. Linkous, Thesis Advisor Date

…….. ……

Dr. Christopher Arntsen, Committee Member Date

…….. …….

Dr. Jennifer Miller, Committee Member Date

…….. …….

Dr. Salvatore A. Sanders, Dean of Graduate Studies Date

# ABSTRACT

Landfill gas (LFG) can be used as a renewable domestic fuel for electricity generation via solid oxide fuel cells (SOFC) based on yttria-stabilized zirconia (YSZ) if species likely to poison the SOFC's anode and passivate the cell are identified, analyzed, and separated.

This work focused on the surface chemistry of methane, the prime constituent of landfill gas.

The methodology for this research was to run a Ni/YSZ/LSM button cell at temperatures of 750 – 900 $^{o}$C with air fed to the lanthanum strontium manganite (LSM) cathode and a reducing gas such as hydrogen fed to the Ni anode before running it on humidified methane gas.

After observing current and voltage transients and obtaining galvanic performance curves under methane, the cell was opened up and analyzed for any contamination of the anode using instrumentation such as scanning electron microscopy (SEM) and energy dispersive spectroscopy (EDS). These results served as the background for similar experiments using landfill gas (containing ~ 50% $CH_4$) obtained from the Mahoning Landfill as fuel. The cell was again run until a steady state was reached, followed by removal and analysis.

Despite the 2- to 2.5-fold water vapor excess, carbon deposition from methane on the anode reduced maximum cell power by 45% in comparison to pure $H_2$. Passivation by LFG gas was even more severe, increasing charge transfer resistance by 654 Ω over simulated LFG at 800 °C and reducing maximum power by 90%.

These results point to trace (< 1%) species besides $H_2S$ and siloxanes having a greater influence on the performance of the SOFC than the methane content of the LFG.

Identifying these contaminants that poison the anode of SOFC cells when run on landfill gas will contribute to developing more efficient and sustainable energy production.

# ACKNOWLEDGEMENT

I want to thank my thesis advisor, Dr. Clovis Linkous, for giving me the opportunity to work on this project. I'm grateful for your knowledge, fatherly guidance, and patience throughout the process.

Even on your extremely busy days and despite having a large research group, you always find the time to help me with the difficult parts of the project and guide me through any obstacles.

I also want to acknowledge the invaluable contributions of Dr. Christopher Arntsen and Dr. Jennifer Miller, who served on my thesis committee. Your encouragement and feedback were critical to the success of this project.

I would like to express my appreciation to Mr. Raymond Hoff for his invaluable assistance with the instruments and analysis of samples during this project. Your extensive knowledge of instrumentation played a crucial role in the success of this project.

I also appreciate the support and help from the entire YSU Chemistry Department.

To my friends and classmates in Dr. Linkous's research group, Geoffrey, Silas, Onyi and Samwel; thank you for making the office hours and lab days enjoyable, and I will miss working with and learning from all of you.

Lastly, I want to thank my family for their unwavering support, encouragement, and tolerance.

# TABLE OF CONTENTS

# LIST OF FIGURES

# LIST OF TABLES

# CHAPTER ONE

# INTRODUCTION

Energy is the foundation of humanity's progress (Elavarasan, 2019), and throughout history, it has aided society in its endeavors. The pursuit of energy with the least cost and pollution is still ongoing and will continue in the future (Elavarasan, 2019). Renewable energy is energy produced from replenishable resources, and efficient use of energy resources is a major topic these days. It is critical to decide which energy source will be employed (Shahzad, 2012). A variety of considerations, including cleanliness, cost, stability, efficiency, and environmental effects, must be considered. Unfortunately, many sectors worldwide continue to rely on fossil fuels for energy generation (Shahzad, 2012). Currently, energy production in some developing countries frequently falls short of energy needs, resulting in frequent power outages. In addition, energy consumption is predicted to rise in tandem with the global economy, and because fossil fuels are finite, it is necessary to examine alternative energy sources, such as renewables, to fulfill future energy demands.

In the 1970s, the United States and the world faced a severe oil shortage that increased interest in alternative energy sources, such as wind power, to generate electricity.As part of the energy reform movement, efforts were made to stimulate domestic oil production, reduce America's dependence on fossil fuels, and find alternative energy sources, such as solar, wind, and nuclear energy (History.com Editors, *Energy crisis (1970s)* 2010).

While maintaining economic progress, environmental protection is quickly becoming one of the most pressing issues in modern economics and science. This is a critical issue from an ecological, social, and economic standpoint (Brodny and Tutak, 2020). The literature demonstrates that substituting renewable energy sources for energy derived from fossil fuels, such as bioenergy,

direct solar energy, geothermal energy, hydropower, wind, and ocean energy (tide and wave), will help the world achieve sustainability over time. Governments, intergovernmental agencies, interested parties, and individuals worldwide anticipate achieving a sustainable future due to the opportunities generated over the past few decades to replace petroleum-derived materials with alternative materials derived from fossil fuels and fuel-based energy sources.

Fossil fuels are, without a doubt, quite successful in terms of power production quality, but they are not advantageous in the long run. Therefore, the industry must transition as quickly as possible to renewable energy sources, as fossil fuels will eventually run out (Shahzad, 2012). Furthermore, these fossil fuels constitute a significant danger to environmental balance and are the source of numerous ecological risks (Shahzad, 2012). Despite substantial efforts at all levels to promote renewable energy as an alternative to fossil fuels, fossil fuels accounted for 73.5 percent of global power production in 2017 (Qazi et al., 2019); renewables accounted for only 26.5 percent of the total. Moreover, according to Qazi et al. (2019), more people need to be aware of renewable energy solutions, which is another significant barrier to their use.

Renewable energy is inextricably related to the natural conditions of each region and locale. Their availability varies significantly from location to location, making it critical to assess their potential to decide their optimal utilization under economically favorable conditions (Gámez et al., 2017). They are the equivalent of fuel for operating the technologies that use them in terms of quantity and quality. It also depends on the energy efficiency and dependability of the technological systems (Gámez et al., 2017). The transition of the global energy industry is accompanied by a shift in the primary fuel types in the energy balance, technological and organizational breakthroughs, and supply chain expansion and optimization. The current stage of the international energy market's evolution is marked by increased energy supply-demand relationships, renewable

energy sources, and energy efficiency. As a result, more financial resources should be applied to the energy sector. However, it should be used to make up for the decline in oil and gas fields' energy production and build infrastructure for traditional and renewable energy sources (Dudin et al., 2019).

## LANDFILL GAS

Biomass is a viable renewable energy source available as wood for combustion, soybeans for biodiesel, corn for bioethanol, and biogas from sewage treatment plants and landfill sites. Landfill gas (LFG) is a natural byproduct produced as organic waste decomposes in landfills. It is primarily composed of methane ($CH_4$), carbon dioxide ($CO_2$), nitrogen ($N_2$), and other minor constituents, such as hydrogen sulfide ($H_2S$) and non-methane organic compounds (NMOCs). LFG is a greenhouse gas (GHG) originating from the anaerobic degradation of municipal solid waste (MSW) landfills. (Ahmed et al. 2015). About 40 to 60 percent of landfill gas is methane, the remainder is mainly carbon dioxide, nitrogen, and a trace amount of other volatile organic compounds (VOCs) make up the rest (<1%), as shown in Table 1.1. In addition, there is a wide variety of species of trace gases, primarily hydrocarbons.

Landfill emissions contribute to global climate change by releasing greenhouse gases such as carbon dioxide and methane. Methane is particularly impactful, with each molecule having 25 times the effect of one carbon dioxide molecule (Bartram, 2020). In the US, landfills for municipal solid waste are the third-largest source of methane emissions, accounting for 15.1% of total emissions (EPA).

Table 1.1 summarizes the composition and percentage average concentration of landfill gas.

Table 1.1: Typical composition of LFG (Hao et al., 2008)

| Constituent Gas | Average concentration (v/v) |
|---|---|
| Methane ($CH_4$) | 50% |
| Carbon dioxide ($CO_2$) | 45% |
| Nitrogen ($N_2$) | 5% |
| Oxygen ($O_2$) | <1 |
| Hydrogen sulfide ($H_2S$) | 100-200 ppmv |
| Halides | 132 ppmv |
| Non-methane organic compounds (NMOCs) | 2700 ppmv |

Since landfill gas flaring harms the environment, it is imperative to devise strategies to capture and utilize it for power generation.

## FUEL CELLS

Fuel cells provide an excellent alternative to utilizing the gases generated in landfill sites to generate electricity. They were discovered over 160 years ago by William Grove. However, despite their superior energy generation efficiency and environmental benefits, they are only now becoming economically viable enough to compete with conventional power generation (Ormerod, 2003).

The fuel cell converts a liquid or gaseous fuel into electrical energy and heat by combining it with an oxidant electrochemically. Compared to the cleanest combustion process, fuel cells emit fewer pollutants, such as NOx, which forms automatically in an air-fed flame, since they operate at less than combustion temperatures (Laosiripojana et al., 2009). Because of its excellent conversion efficiency and environmental acceptability, the fuel cell is acknowledged as an efficient means of producing energy from chemical components (Laosiripojana et al., 2009). Unlike most batteries, fuel cells require a continuous source of fuel and oxygen (usually air) to sustain the chemical

reaction. In a battery, the chemical energy is commonly derived from metals and their ions or oxides that are already present, except in flow batteries. Therefore, fuel cells can continuously produce electricity if oxygen and fuel are available. Furthermore, because it is free of moving parts, lubrication, wear, leakage, and heat loss issues that plague traditional heat engines are avoided. This technology provides flexibility and adaptability (Ormerod, 2003).

Over the years, different types of fuel cells have been developed. However, their operating principle is the same as shown in Figure 1.1.

Hydrogen + Oxygen = Water + Electrical power and Heat

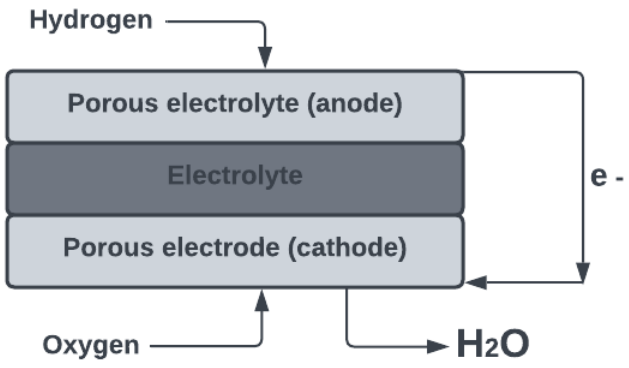


Figure 1.1: Schematic diagram showing the general operating principles of a fuel cell

Fuel cells contain an anode, a cathode, and an electrolyte that allows ions, typically positively charged hydrogen ions (protons), to move between them. Fuel undergoes oxidation reactions in the anode that generate ions (often positively charged hydrogen ions) and electrons. An electrolyte transports ions from the anode to the cathode. Electrons flow from an anode to a cathode through an external circuit to create direct current electricity. At the cathode, ions, electrons, and oxygen

react to form water and possibly other products. Fuel cells are linked in series to achieve a higher output voltage. An interconnecting plate is always fitted to allow electronic contact between the anode of one cell and the cathode of the next cell (Laosiripojana et al., 2009).

## SOLID OXIDE FUEL CELLS

Unlike other fuel cells, solid oxide fuel cells (SOFC) are a form of high-temperature fuel cells that look to be one of the most promising technologies for producing efficient and clean energy for various applications (Laosiripojana et al., 2009). SOFCs are a mature technology capable of achieving 60% electrical efficiency. The efficiency of SOFCs makes them particularly suitable for off-grid applications since they can deliver energy and heat. However, concerns about endurance, particularly when utilized dynamically, and the high initial cost remain the main barriers to the broader adoption of this technology (Baldi et al., 2019).

A solid oxide fuel cell typically has four layers: (i) anode, (ii) electrolyte, (iii) cathode, and (iv) interconnect. All the segments in the cell are made up of ceramics or high temperature alloys. Air enters the cathode, and fuel enters the anode. At the cathode, oxygen is reduced by absorbing electrons and forming lattice $O^{2-}$ (Afroze et al., 2020).

Figure 1.2 shows oxygen ions flow through the electrolyte to reach the anode. Therefore, when the fuel enters the anode, it reacts with oxygen, releasing heat, water and electrons. First, the electrons will go to the external circuit and generate power; then, they will enter the cathode to reduce more $O_2$. By repeating these cycles continuously, power is generated, and the whole SOFC circuit is completed. (Afroze et al., 2020).

The commonly used electrolyte is yttria-stabilized zirconia (YSZ) due to its high chemical and mechanical stability and high ionic conductivity.

The YSZ functions at high temperatures, often between 750 and 1000 $^{o}$C (Ormerod, 2002).

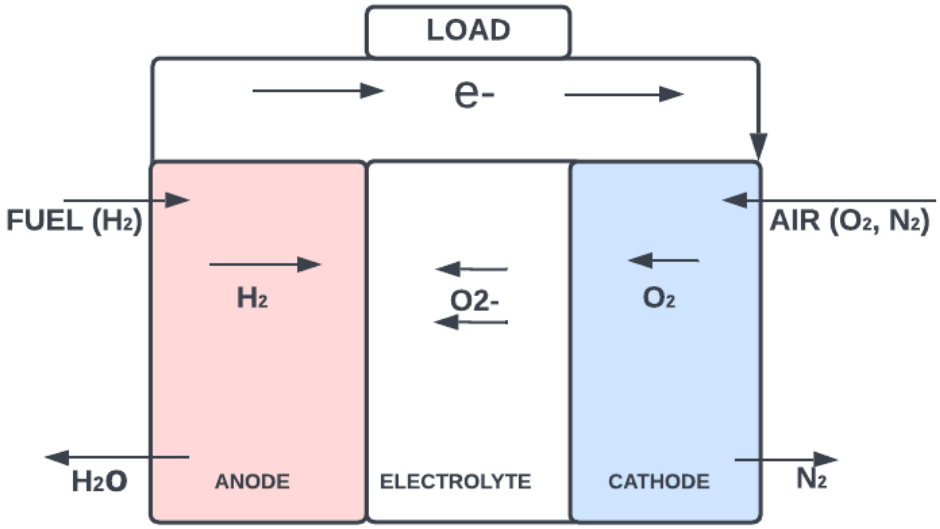


Figure 1.2: Schematic diagram of a solid oxide fuel cell

The equations below show the electrode reactions and the overall cell reaction.

Cathode: $O_2 + 4\ e^- \longrightarrow 2\ O^{2-}$

Anode: $2\ H_2 + 2\ O^{2-} \rightarrow 2\ H_2O + 4e^-$

Overall: $2\ H_2 + O_2 \rightarrow 2\ H_2O$

## PROBLEM STATEMENT AND OBJECTIVE

The volume of trash generated every year in the US is enormous. About 728,000 tons of garbage are generated daily, enough to fill 63,000 garbage trucks (*Land of Waste: American Landfills and Waste Production*). Rather than allowing this waste to be a nuisance to the environment or just burning off the biogas generated in these landfill sites, it is essential to develop an efficient system to utilize these landfill gases and turn them into valuable products. Due to the constant demand for local energy in our society today, fuel cells have been identified as one of the efficient ways to utilize these gases as a better alternative when compared to combustion engines, as fuel cells emit little or no pollutants with an efficiency of up to 60%. In addition, solid oxide fuel cells operate at a very high temperature of about 750 °C, eliminating the need for precious metal catalysts and thereby reducing cost. Unlike other fuel cells, SOFCs are less prone to carbon monoxide poisoning, can tolerate a modest amount of sulfur, and can reform fuel internally, given a sufficient water vapor pressure.

There are different types of fuel cells ranging from proton exchange membrane (PEM) fuel cells, alkaline fuel cells (AFCs), phosphoric acid fuel cells (PAFCs), molten carbonate fuel cells (MCFCs), and SOFCs. However, the general operation of fuel cells follows the same principle.

Over the years, solid oxide fuel cells have received significant attention globally, not excluding the Linkous research lab students at Youngstown State University who have done several investigations on SOFC, which involves investigating the effects of hydrogen sulfide in landfill gas on SOFC anode poisoning (Khan, F. 2012). Khan concluded that landfill gas must be pretreated to reduce the sulfur content from over 100 ppm down to single digits or less to sustain SOFC operation at 750 $^{o}$C.

Also, *The Effects of Siloxanes on Solid Oxide Fuel Cell Performance (Zivak, M. 2020)* were studied. Zivak demonstrated that a cell operated on pure dry hydrogen gas gave a lower voltage when the siloxane concentration is increased from 5 ppmv to 10 ppmv.

She found that humidifying the hydrocarbon fuel prevents silica deposits on the cell's anode. However even after removing sulfur and siloxanes, the cell failed to reach the expected voltage and current output when she experimented with humidified Mahoning Landfill gas. As a result, it had to be concluded that there was yet another contaminant causing the cell performance degradation.

A working hypothesis was developed where methane and other hydrocarbons were pyrolyzing onto the electrode surface, depositing carbon and blocking further reaction:

$CH_4(g) \longrightarrow C(s) + 2\ H_2$

The intent of humidifying the methane was to prevent pyrolysis through a steam reforming reaction:

Water gas: $C + H_2O \rightleftharpoons CO + H_2$

Water gas shift: $CO + H_2O \rightleftharpoons CO_2 + H_2$

Therefore, this research primarily focuses on running an SOFC on high purity, humidified methane so as to understand its characteristics, and then switch to real LFG to see if the electrochemical performance is sustained. A positive response would indicate that SOFC performance is limited by the surface chemistry of $CH_4$ on the Ni anode.

The aim is to study the stability and performance of solid oxide fuel cells (SOFCs), specifically Pt/YSZ/Pt and Ni/YSZ/LSM button cells, operated in different gases and at different temperatures.

The platinum-coated button cell is an ideal material for studying the SOFC response to impurities because it has a high activity for the oxygen reduction reaction (ORR) and high stability under the harsh operating conditions of an SOFC. The high activity of platinum enables the cell to operate at high currents and generate a large amount of electrical power. In addition, the high stability of platinum ensures that the catalyst remains active and does not degrade over time, allowing the cell to operate for extended periods.

This research will be accomplished in several steps, as highlighted below:

In the first stage, the Pt/YSZ/Pt button cell will be run on hydrogen and humidified methane gas at different temperatures to establish the cell's stability and response to methane fuel relative to $H_2$.

In the second stage, the plain YSZ button cell and a coated Ni/YSZ/LSM anode will be analyzed using surface-sensitive instrumentation to determine their elemental composition and morphology, which will serve as the background for comparison in the later stages of the experiment.

In the third stage, the Ni/YSZ/LSM will be run on hydrogen and humidified methane gas at different temperatures and conditions so as to achieve steady operation, and the reduced cell will be analyzed using surface-sensitive instrumentation to determine how the anode surface may have been altered particularly by carbon.

In the fourth stage, the Ni/YSZ/LSM will be run on landfill gas, noting steady state or continuous decay behavior, and analyzed using surface-sensitive instrumentation to compare the results with the analysis done in stage three. This comparison will help determine any new elements or compounds that may have been added and their effect on the cell's performance.

Overall, the results of this experiment will provide valuable information on the stability and performance of SOFCs when operated in different gases, particularly landfill gas, at different temperatures, and will help to advance the development of this technology for practical applications in the future.

# CHAPTER TWO

# INSTRUMENTATION, MATERIALS, AND EXPERIMENTAL PROCEDURE

The following instruments were used to achieve a stabilized cell to study its behavior under different gases and at different temperatures to generate the voltage-current time plot for the cell.

## PROBOSTAT™

The ProboStat™ system can be used to test the performance and durability of fuel cell components, including catalysts, membranes, and electrodes, under high-temperature conditions of up to 1600 $^{o}$C under controlled conditions. It was developed and tested in the Kofstad/Norby group at the University of Oslo. The system features a versatile construction and a broad range of accessories. Inorganic materials, electroceramics, fuel cell components, membrane materials, etc., can be studied, characterized, and tested. (*https://norecs.com/)*

The ProboStat™ system is an essential tool for fuel cell research and development, providing valuable information on the electrical properties, transport parameters, and kinetics of fuel cell components and systems at high temperatures. Although it has many applications, our focus is on testing fuel cell components and single (button) cells. (*Probostat Versatile high-temperature test fixture*).

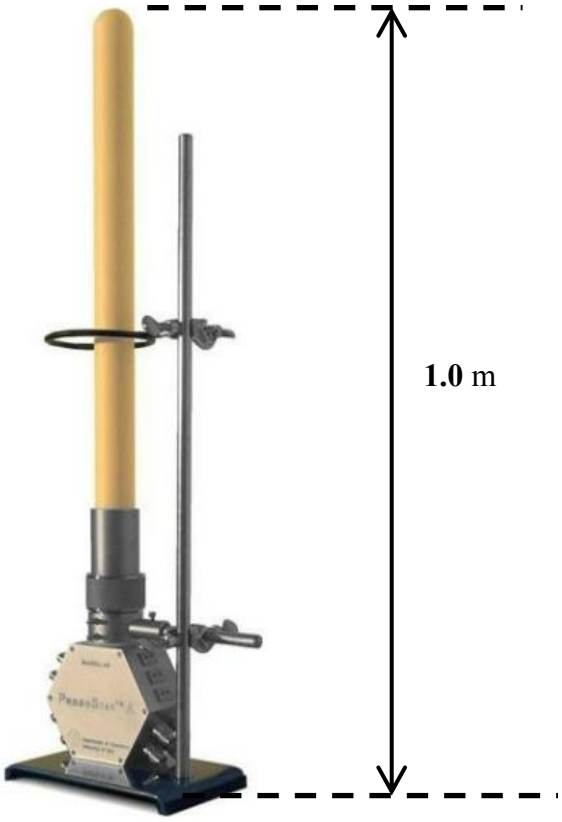


Figure 2.1 is a pictorial representation of the Probostat instrument and its approximate height.

## YSZ BUTTON CELL

The YSZ button cell is an essential component in a solid oxide fuel cell (SOFC) and is composed of three main components: The yttrium stabilized zirconium (YSZ) electrolyte, the nickel/YSZ cermet anode, and the lanthanum strontium manganite ($La_{0.9}Sr_{0.1}MnO_3$) cathode.

The YSZ electrolyte is the central component that enables oxygen ion conduction and is sandwiched between the anode and cathode, as shown in Figure 2.2. It is important to note that the SOFC must be operated at a high temperature, typically above 750°C, to achieve sufficient ion conduction.

A sealant such as Ceramabond is applied with a spatula on a clean surface of the button cell holder before fixing the button cell on it and allowed to cure in hot air. This step is crucial in maintaining an air-tight system by separating the gaseous fuel from oxygen which is essential to generate electricity. If the two gases were allowed to mix, the SOFC would not achieve the estimated thermodynamic voltage and, above a certain concentration, run the risk of ignition.

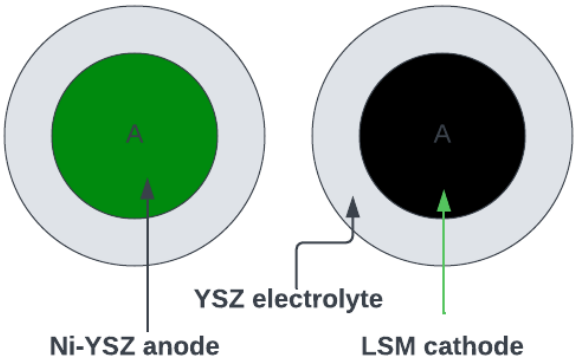


Figure 2.2: YSZ button cell

After the experiment, a Dremel tool is used to remove the sample and prepare support tube for the next sample.

## MASS FLOW CONTROLLER

The Brooks mass flow controller controls the flow of gases delivered to the compartment of a button cell depending on the setpoint, which ranges from 0-100 mL/min. The controller has a mass flow sensor, a proportional control valve, an inlet, and an outlet valve for gases, which connects to the gas and to the instrument to which the gas is channeled. The digital display of the controller is where the setpoint for gases can be adjusted to monitor the rate of flow of the gases. Mass flow controllers require a specific pressure range for gas or liquid supply. If the pressure is too low, the mass flow controller will suffer from a lack of fluid and will not achieve its set point. Conversely, high pressure may lead to erratic flow rates. The indicator light changes from red to green when the setpoint is attained.


Figure 2.3: Mass flow controllers and display unit

## HUMIDIFYING COMPARTMENT

This glass vessel is filled to the level mark with water maintained at 89 degrees (vapor pressure = 506 torr, or 67% humidity) so as to ensure a stoichiometric amount of water vapor to shift convert the methane to hydrogen:

$CH_4 + 2\ H_2O \rightleftharpoons CO_2 + 4\ H_2O$

There is a risk of water condensation at higher vessel temperatures and humidity levels, which can clog the gas lines and give erratic cell performance. At lower temperatures and relative humidity, there may not be sufficient water vapor to prevent pyrolytic decomposition of the methane.

The humidifying vessel has an inlet and outlet for gases and a compartment for the thermocouple that measures the water temperature. The bath is connected to a variable controller, which helps to heat the bath and maintain its temperature based on the set point value temperature of the controller as shown in Figure 2.4. The methane gas enters through the vessel's inlet to the water bath and combined with the water vapor in a ratio of 1 to 2 parts, is humidified for subsequent conversion to hydrogen gas that serves as fuel for the anode of the button cell. The outlet from the humidification vessel also has a heating tape wound around the discharge tubing to ensure the vapor does not condense as it travels to the instrument.

The following reactions take place in the SOFC once the methane is humidified:

$CH_4 + H_2O \longrightarrow 3\ H_2 + CO$

$CO + H_2O \longrightarrow H_2 + CO_2$

$CH_4 + 2\ H_2O \longrightarrow 4\ H_2 + CO_2$

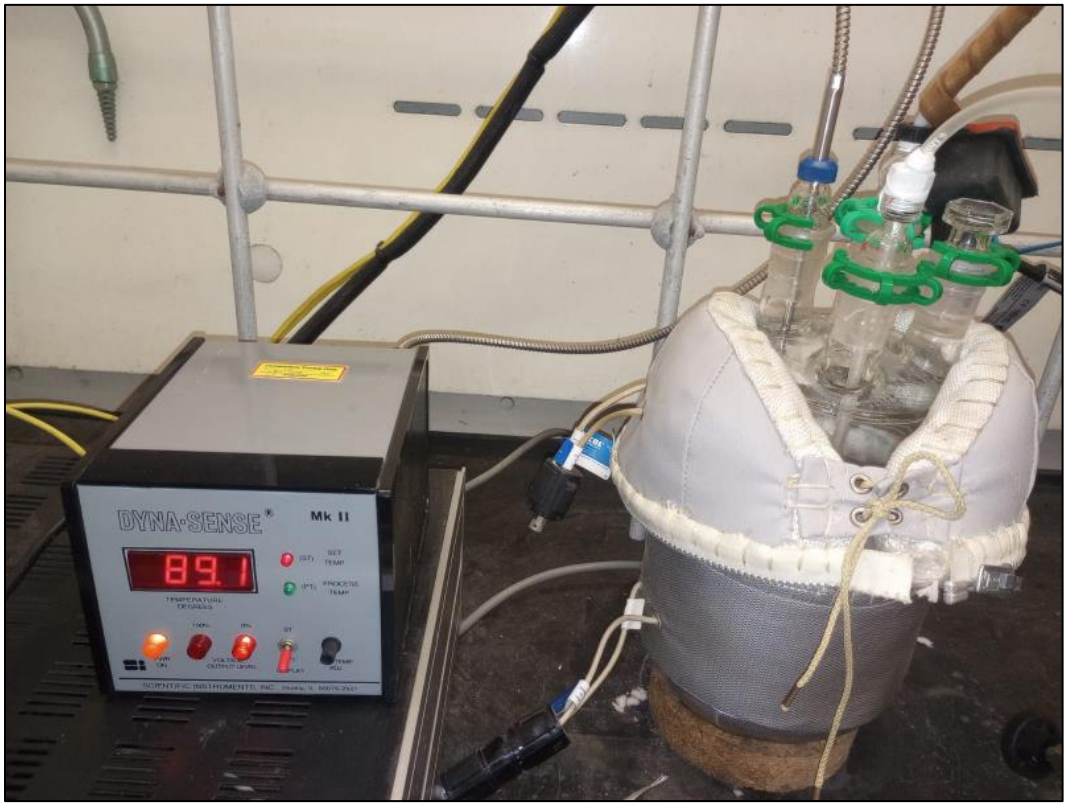


Figure 2.4: variable controller (l) and humidifying vessel (r)

## MULTIMETERS

A multimeter is a standard tool that can be used to measure the voltage output and current of a solid oxide fuel cell (SOFC). The multimeter is an electronic device that measures voltage, current, and resistance, among other electrical quantities.

The accuracy and range of a multimeter will vary depending on its specific model and specifications. Some multimeters are designed for general use that may not have the accuracy or range necessary for precise measurements of SOFCs. To accurately measure the voltage and

current output of the cells, high-precision voltmeters or current meters may be required as shown in Figure 2.5.

For this research, the multimeters used are The Hewlett Packard (HP) 3478A multimeter, Fluke 73 series II multimeter, and Velleman DV 890 multimeter, which were available in the Linkous research lab.


Figure 2.5: Multimeters

## X-RAY DIFFRACTION (XRD)

The X-Ray Diffraction (XRD) technique can be used to characterize a wide range of materials, such as metals, ceramics, polymers, and biomolecules. It works by firing a beam of X-rays at a sample and measuring the diffracted or scattered X-rays produced. The pattern of diffracted X-rays is unique to each material and can be used to identify the type and arrangement of atoms within the sample. This experiment used the Bruker AXS X8 Prospector diffractometer in the

Youngstown State University X-Ray Diffraction Laboratory to determine the sample's composition.

## SCANNING ELECTRON MICROSCOPY (SEM) AND ENERGY-DISPERSIVE X-RAY SPECTROSCOPY (EDS)

A combination of scanning electron microscopy (SEM) and energy-dispersive x-ray spectroscopy (EDS) is a powerful analytical technique used to study materials at the nanoscale (Brostrøm et al., 2020). An SEM works by directing a beam of high-energy electrons at a sample, which results in secondary electrons being emitted from the surface (Baguer, 2005). These electrons are then detected and used to produce an image of the sample's surface (Sammer et al., 2008). EDS is used in combination with SEM to determine the chemical composition of the sample by measuring the energy of X-rays emitted by the sample when electrons bombard it from the SEM. The X-rays are unique to each element, and their energy can be used to identify the elements in the sample. Metals, ceramics, polymers, and biomolecules can be characterized non-destructively using SEM and EDS technology. It is widely used in materials science, pharmaceuticals, and environmental science.

In a typical SEM/EDS system, the sample is placed in a vacuum chamber and bombarded with electrons from an electron gun. The resulting secondary electrons and X-rays are collected and analyzed to produce images and compositional data (*Measurlabs.com, "SEM-EDX Analysis").*

The SEM/EDS instrument used for the analysis of the samples is a JEOL JIB-4500.

# METHODOLOGY

The method employed for this research is to mount the button cell on the sample support tube with the ceramic sealant and air-dry it at room temperature for 4 hours, as shown in Figure 2.6. The sealant used is the Aremco Ceramabond.

This step is necessary to keep a gas-tight system to prevent the two gases (fuel and oxidant) from mixing.

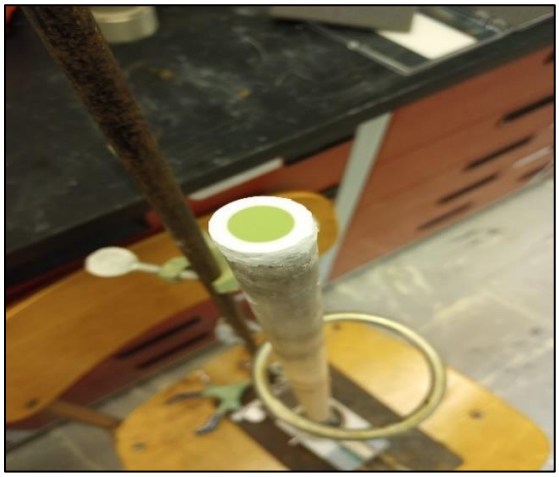

Figure 2.6: Diagram of a button cell attached to the sample support with Ceramabond.

Next is to mount the inner gas supply tube to the gas inlet at the top of the base, then connect the electrode contact pair to the internal electrical feed-throughs. Figure 2.7 is the top view of the electrical contact points in the Probostat instrument for the anode and cathode gas supplies. The dotted spots are the specific points of electrode connection in the device.

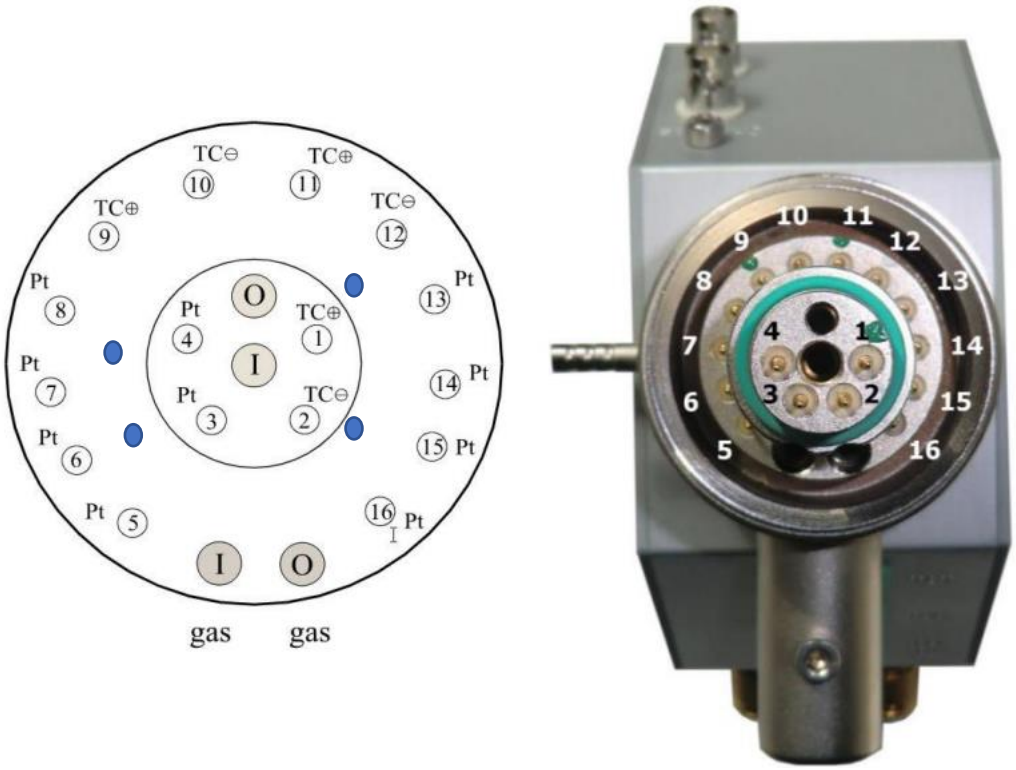


Figure 2.7: Internal electrical contacts of the Probostat (Norecs. (n.d.); 2023)

Next is to slide the sample support tube bearing the mounted cell over the inner gas supply tube, ensuring the cell's cathode side makes good contact with the platinum mesh on the top of the gas inlet for good electrical connectivity.

Then connect the other electrode contact pair and add the spring compression system to the Probostat base.

The assembled Probostat is covered and fastened with a screw collar, and placed in a vertical tubular furnace, as shown in Figure 2.8

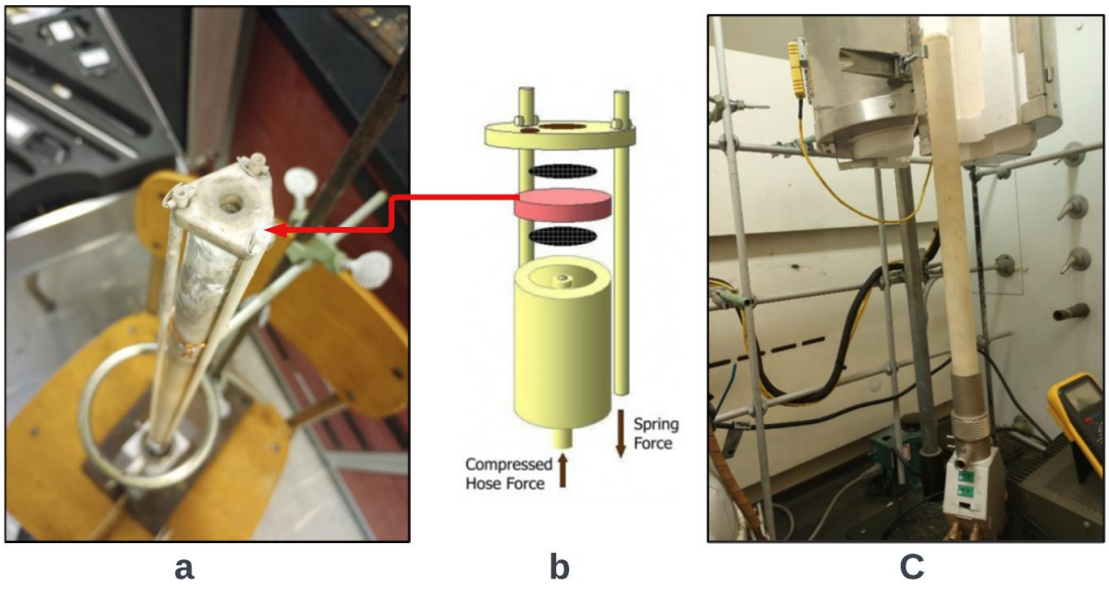


Fig. 2.8a: Probostat assembly, Fig. 2.8b: Button cell with spring loading, 2.8c: The Tubular Furnace with Probostat assembly (Probostat Button Cell fixture 2022)

The furnace temperature control button is adjusted to the desired temperature and is allowed to heat up gradually until the setpoint temperature is attained. The resistance across the cell is measured with a multimeter connected across the Probostat. As the cell is heated up in the furnace, the resistance starts to fall gradually to the minimum, which indicates that the cell is conductive, and the gases can be introduced at this point to the cell anode and cathode. The Brooks mass flow controllers control the gas flow rates at a set point of 50 ml/min.

## Pt/YSZ/Pt BUTTON CELL SAMPLE PREPARATION

The plain YSZ button cell is coated with platinum ink on both sides (anode and cathode), smeared to remove void volume, and air-dried. The cell is then gradually heated in an oven to 1000 $^{o}$C and maintained at that temperature for 4 hours to allow for complete sintering of the particles.

After sintering, the cell is cooled to room temperature and checked for conductivity using a multimeter by placing its probe on the cell surface. Finally, the cell is mounted on the sample-bearing rod of the Probostat with Ceramabond and allowed to dry in the air.

Figure 2.9(a): The plain YSZ button cell and (b) coated with platinum ink

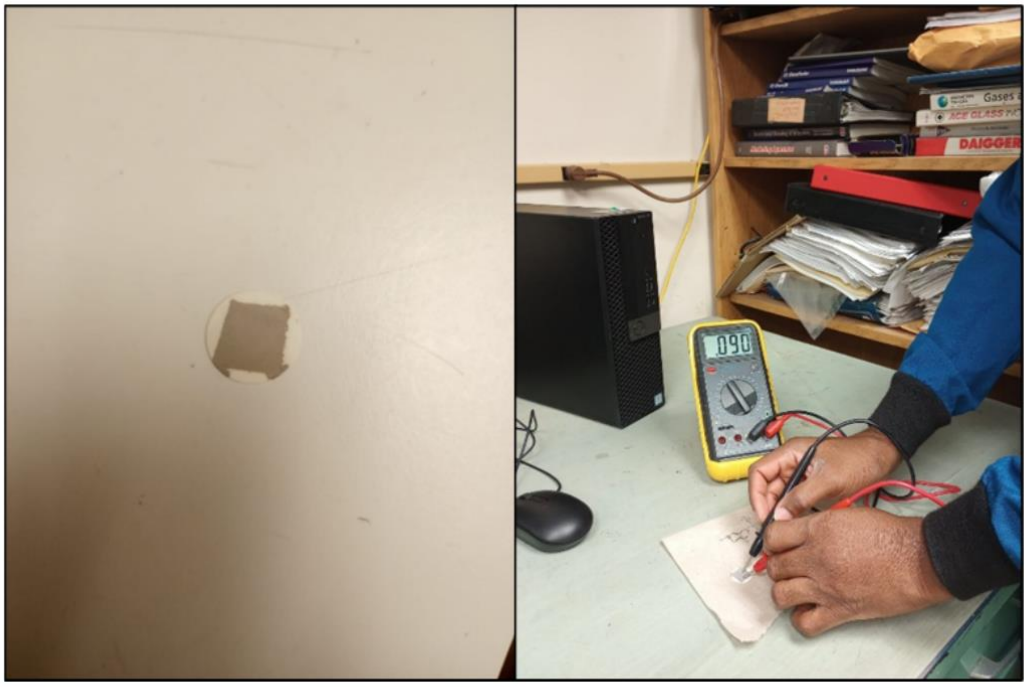

Figure 2.10: The coated YSZ button cell with platinum on both sides and testing for its conductivity using the multimeter

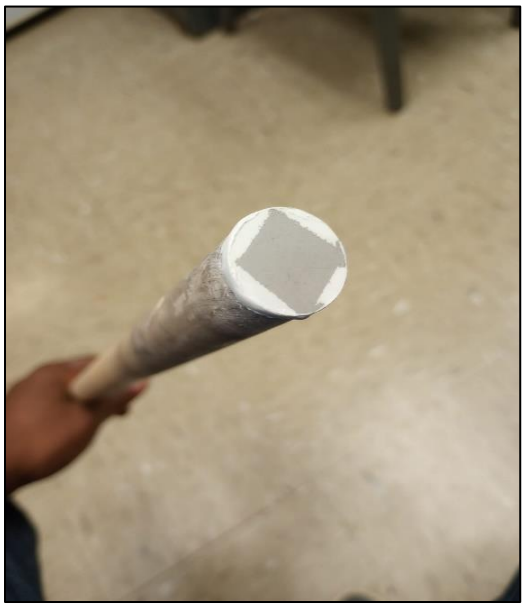

Figure 2.11: The mounted cell on the sample bearing rod of the Probostat using Ceramabond

The mounted cell assembly in the Probostat is heated up to 750 $^{o}$C with oxygen in pressurized air sent to the cathode and hydrogen as fuel for the anode until a steady state is attained. The hydrogen is replaced with argon gas to purge the system of any residual hydrogen, which could cause a risk of explosion, and helps stabilize the system before introducing the methane. The methane is humidified by connecting it through a humidifying vessel and allowed to run until a steady state is attained. A load is imposed on the system with a load box resistor, with the ammeter connected in series and the voltmeter in parallel with the cell. A voltage and current time plot can be generated, which provides information about the performance of the fuel cell.

## Ni/YSZ/LSM BUTTON CELL SAMPLE PREPARATION

Due to the short supply of the coated Ni/YSZ/LSM button cells and a lack of information on its exact composition, Ni-coated YSZ button cells were fabricated in-house using a formulation prepared by former student Feroze Khan, which is 40 % NiO - 60 % YSZ by weight, diluted with α-terpineol of density 0.93 g/mL added to the cermet powder in order to achieve a desired consistency and reconstitute it into a paste for the anodic side of the cell. The LSM ink available in the lab (fuelcellmaterials) was used for the cathodic side of the button cell.

Figure 2.12: Ni cermet formulation diluted with α-terpineol.

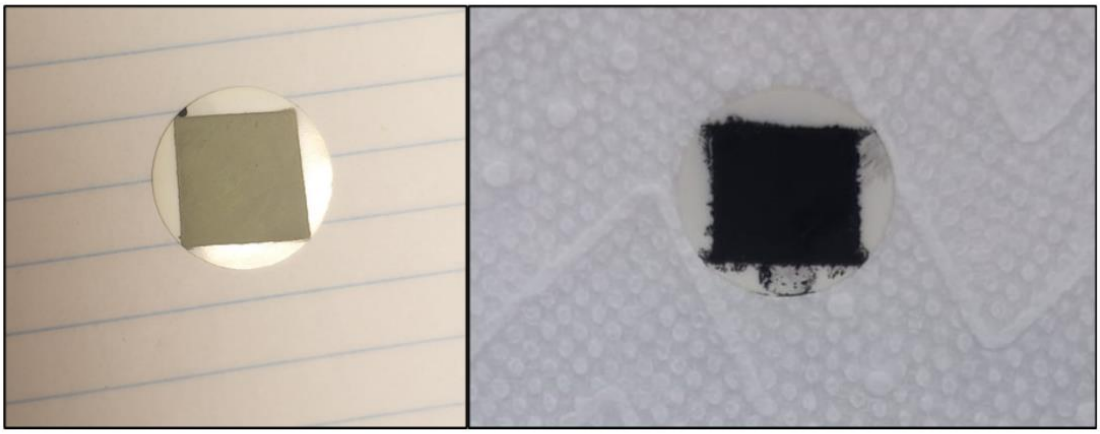

Figure 2.13: Ni/YSZ Anode (before reduction) and LSM Cathode.

The button cell is mounted on the sample-bearing tube of the Probostat. The mounted cell assembly is first run with air as the cathode oxidant and hydrogen as the anode fuel until a steady state is attained. This process helps to reduce the nickel oxide into metallic nickel before following it up with argon gas for about 10 min to purge the system of any residual hydrogen, which can be a safety hazard, and stabilize the system before introducing the methane through a humidified vessel. The fuel cell's performance can be determined by measuring the cell voltage and current with a voltmeter in parallel and an ammeter connected in series with the Probostat, as shown in Figures 2.14 and 2.15.

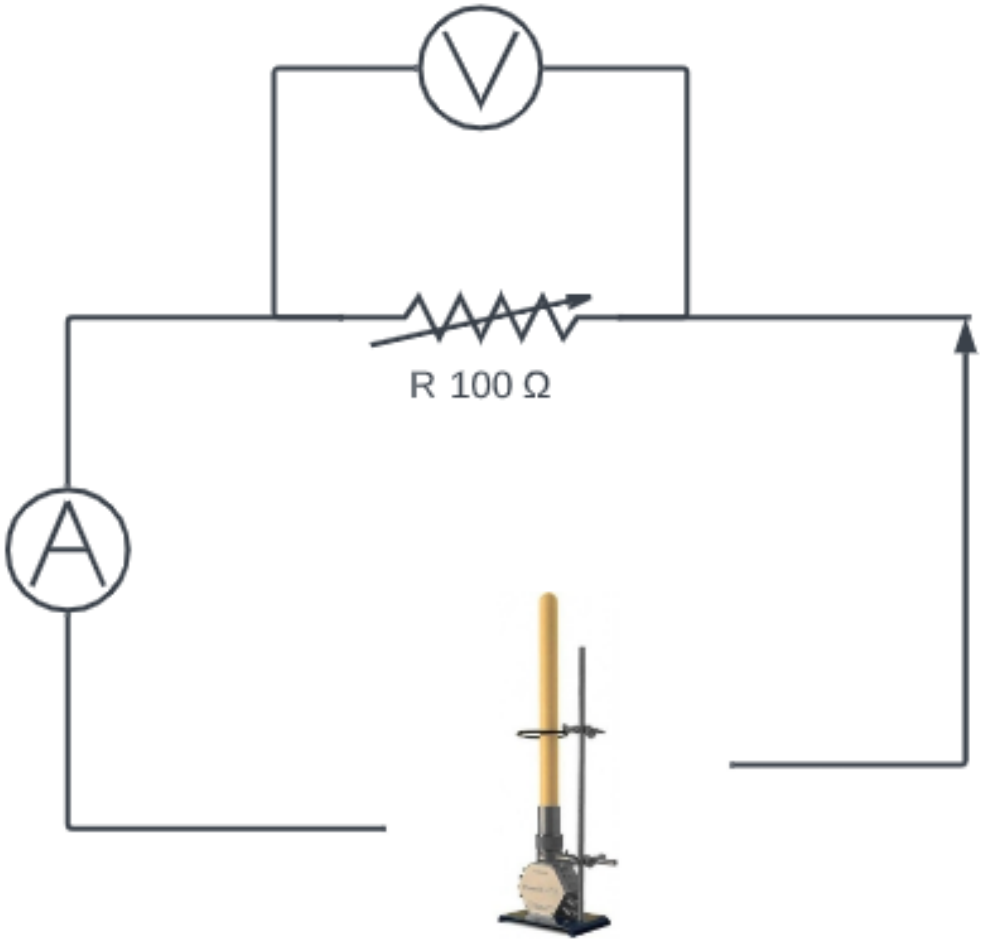


Figure 2.14: The load box resistor, ammeter, and voltmeter connected in series with the Probostat.

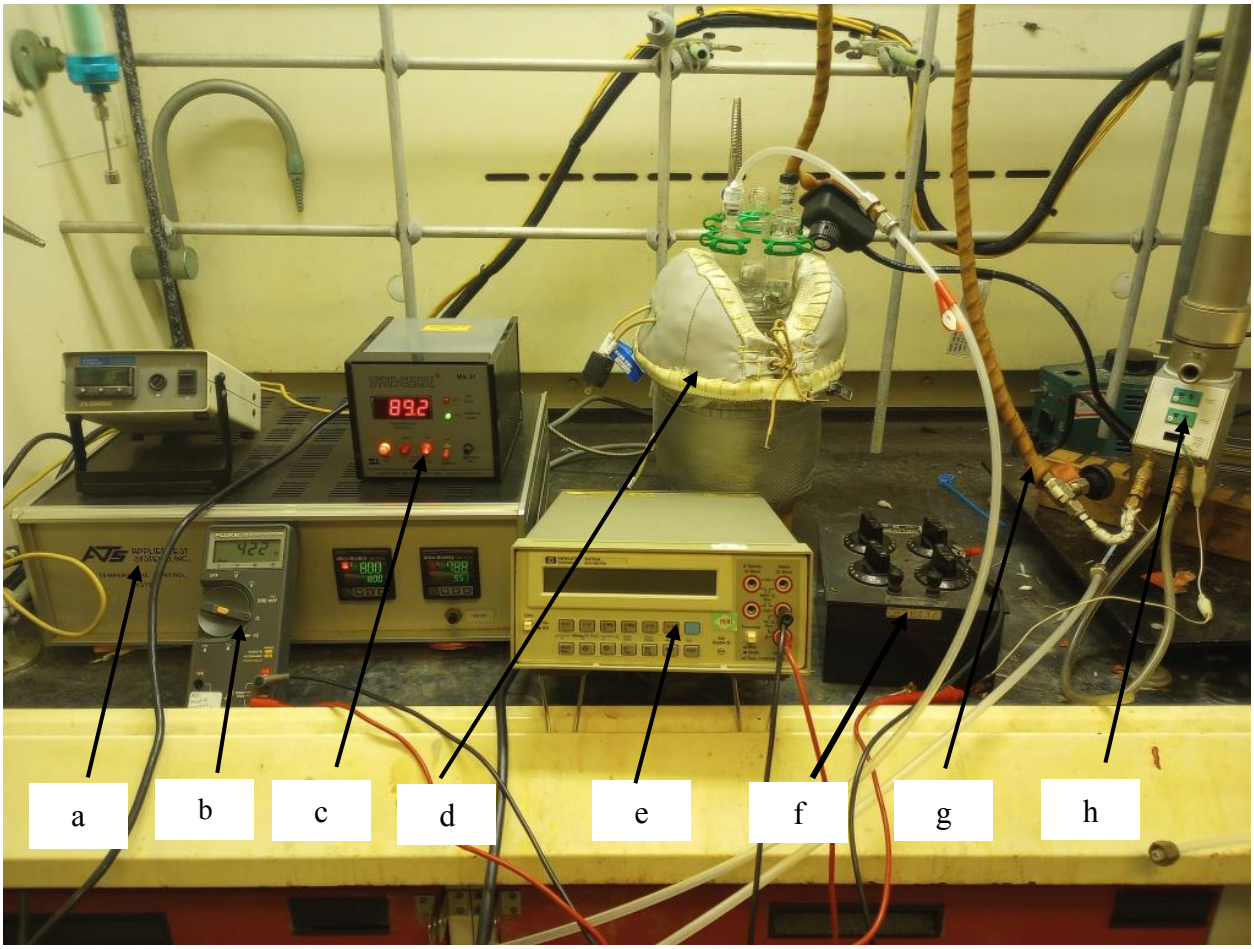


Figure 2.15: The cell assembly with ammeter, voltmeter, and a load box.

a. furnace power supply

b. voltmeter

c. temperature controller for gas humidifier

d. humidifier vessel

e. ammeter

f. load box

g. hot gas /water vapor line connecting humidifier to anode chamber of the SOFC

h. Probostat containing the SOFC

# CHAPTER THREE

# RESULTS AND DISCUSSION

## ELEMENTAL ANALYSIS OF COATED Ni/YSZ/LSM BUTTON CELL

To determine the elemental composition of the in-house fabricated button cell, XRD analysis was carried out on a fresh sample substrate, and the result was compared to the value in the literature, as shown in Figures 3.1 and 3.2.

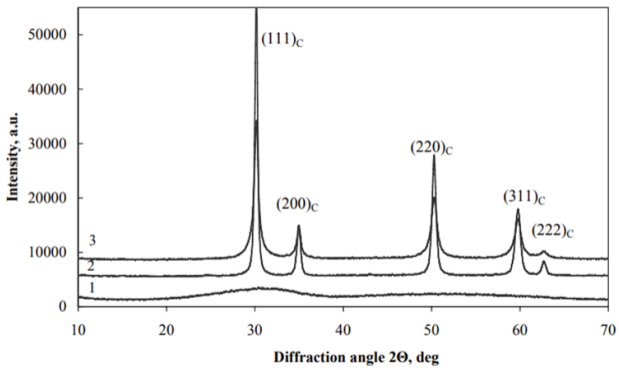


Figure 3.1: XRD of YSZ button cell (Brinkienė & Cėsnienė et al, 2008).

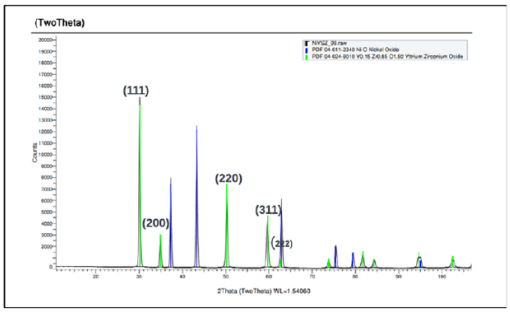


Figure 3.2: XRD of Ni/YSZ button cell fabricated in-house

According to Figure 3.2, the green peaks match the crystalline planes of YSZ compared to those obtained in the literature, as shown in Figure 3.1. The blue peaks that are not labeled correspond to the NiO. This confirms that the composition of the fabricated button cell anode is Ni/YSZ.

This XRD data regarding the surface of the Ni/YSZ anode, along with other techniques, can serve as a reference point for comparing the composition of the button cell before and after exposure to methane gas. This will allow us to detect any contaminants, such as carbon, accumulated on the anode of the cell and determine their impact on its performance.

An SEM/EDS analysis was performed on the substrate. The results of this analysis are shown in Figure 3.3 and Table 3.1.

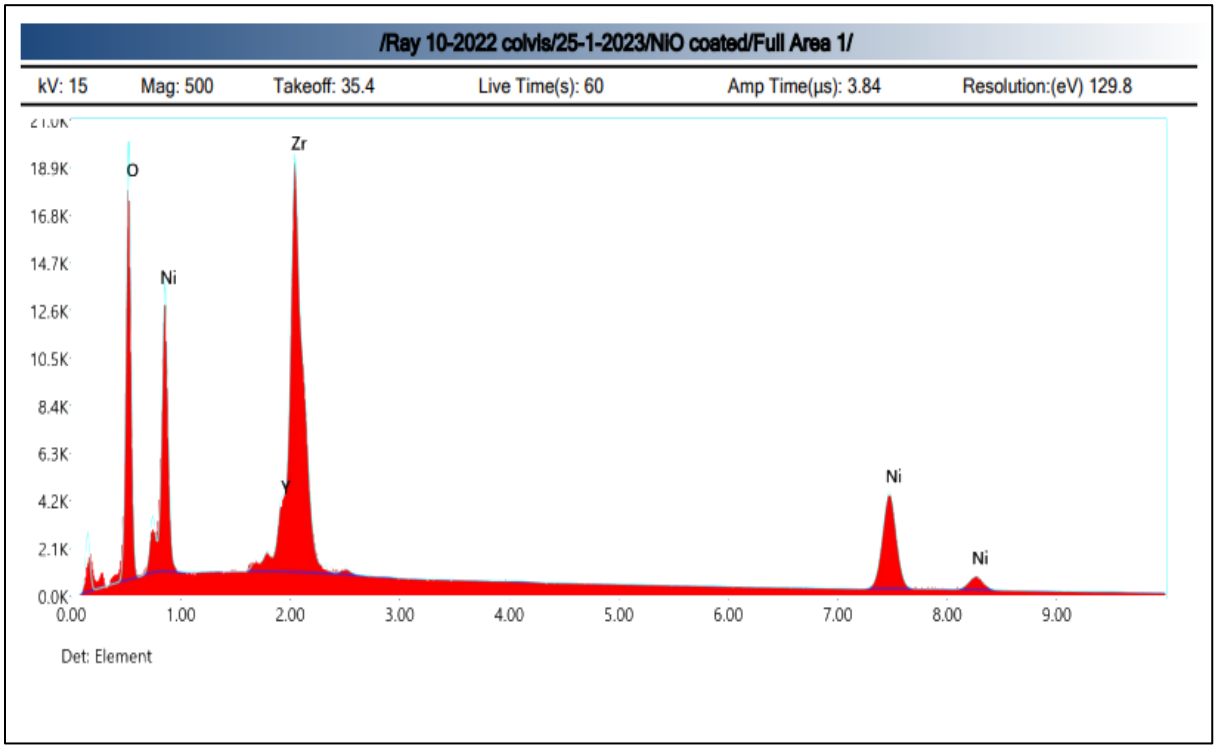


Figure 3.3: SEM/EDS of Ni/YSZ button cell fabricated in-house.

Table 3.1: SEM/EDS DATA OF ELEMENTAL COMPOSITION OF SOFC ANODE

| Element | Weight % | MDL | Atomic % | Error % |
|---|---|---|---|---|
| $O_K$ | 28.91 | 0.35 | 64.56 | 9.64 |
| $Ni_K$ | 34.75 | 2.39 | 21.15 | 3.71 |
| $Y_L$ | 5.2 | 0.46 | 2.09 | 6.09 |
| $Zr_L$ | 31.14 | 0.48 | 12.19 | 4.6 |

Figure 3.3 indicates the presence of nickel, yttrium, and zirconium peaks, while Table 3.1 shows that the substrate contains 34.75% by weight of nickel. This percentage is lower than the 40% by

weight specified in the Feroze Khan recipe , but it still confirms that the button cell has nickel on its surface.

## Pt/YSZ/Pt BUTTON CELL RUN ON HYDROGEN AND AIR AT 750 °C

The cell is first run on hydrogen as the fuel for the anode while air is delivered to the LSM cathode compartment of the cell. Figures 3.4 and 3.5 show the voltage-time and the current-voltage plots, respectively.

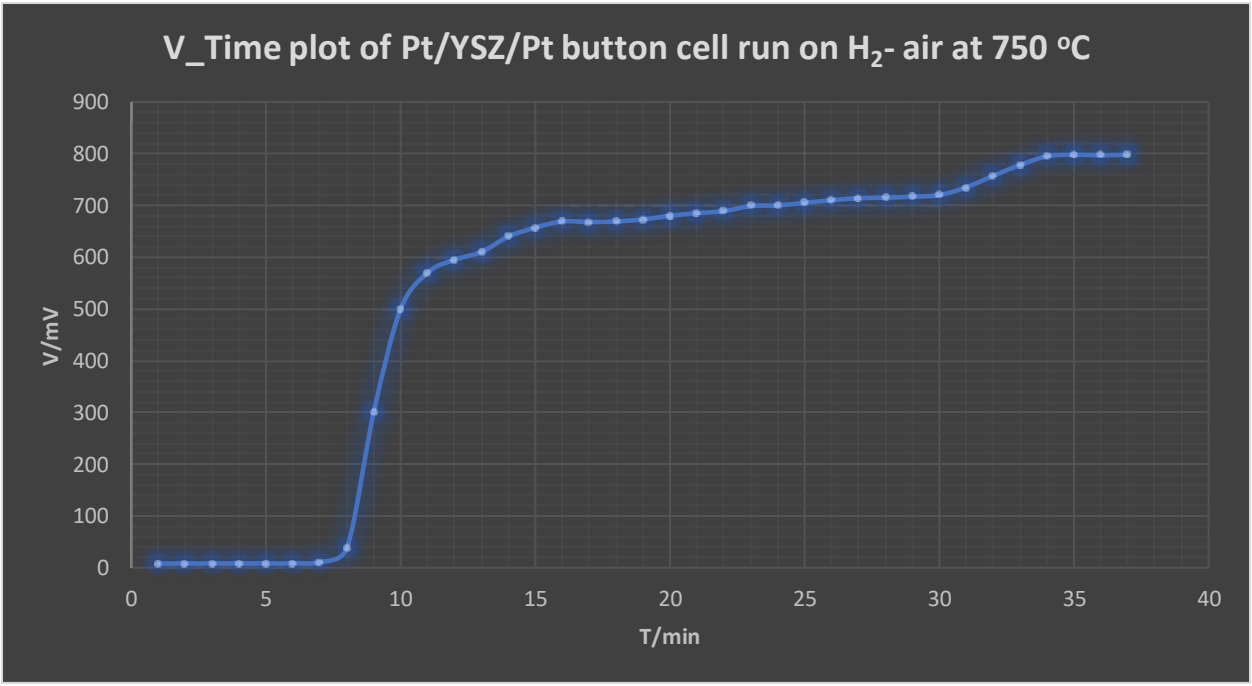


Figure 3.4: V_Time plot of the Pt/YSZ/Pt run on hydrogen and air at 750 °C and 100 Ω load resistor.

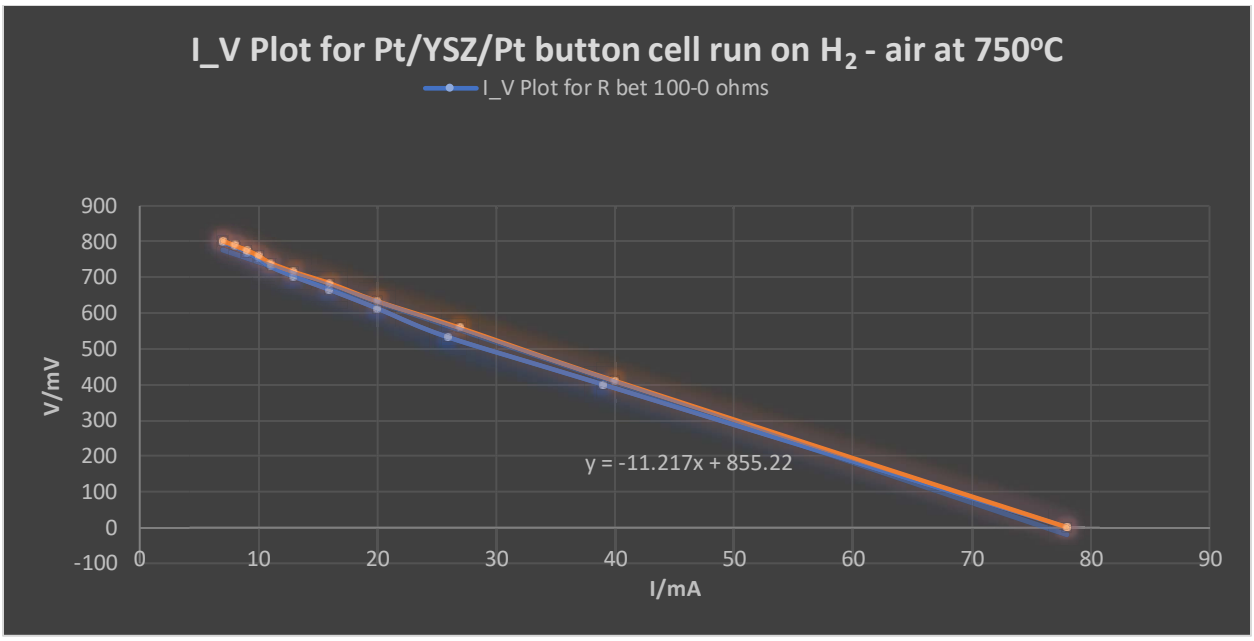


Figure 3.5: I_V plot of the Pt/YSZ/Pt run on hydrogen and air at 750 °C.

The voltage-time graph in Figure 3.4 shows a steady increase in voltage to a steady state value of 798 mV after 35 min.

The current-voltage graph in Figure 3.5 is a plot of two separate curves that show the performance of the button cell at 750 °C. With a load of 100 Ω imposed on the cell assembly at steady state, the cell attained a maximum voltage of 798 mV and a current of 7.0 mA. The load box resistor is varied from 100 to 0 Ω and back until successive currents and voltages are obtained. The orange dots almost perfectly fall on the blue dots, showing that the cell is responsive in the same manner and at a steady state as the load is dialed up and down.

From Ohm's law (V=IR) and the linear nature of the performance curve, the resistance of the cell can be calculated, which is also the slope of the line under the graph. The resistance is estimated to be 11.2 Ω and the maximum power produced by the cell is 16400 $\mu$W which also shows good electrical contact between the button cell and the Probostat.

## RESISTANCE OF A YSZ BUTTON CELL

The resistance offered by the YSZ button cell can be estimated to find out how it compares with the slope (resistance) of the cell, which can be calculated as shown below.

$R = \rho\, l/A$

Where R is the resistance of the YSZ button cell

$\rho$ is the resistivity of the YSZ button cell

$l$ is the thickness of the YSZ button cell

$A$ is the active area of the YSZ electrolyte in contact with the electrodes.

The resistivity of the YSZ button cell electrolyte run at a temperature of 800 $^{o}$C can be read from Figure 3.6 which is given as 4 x $10^{1}$ Ω cm.

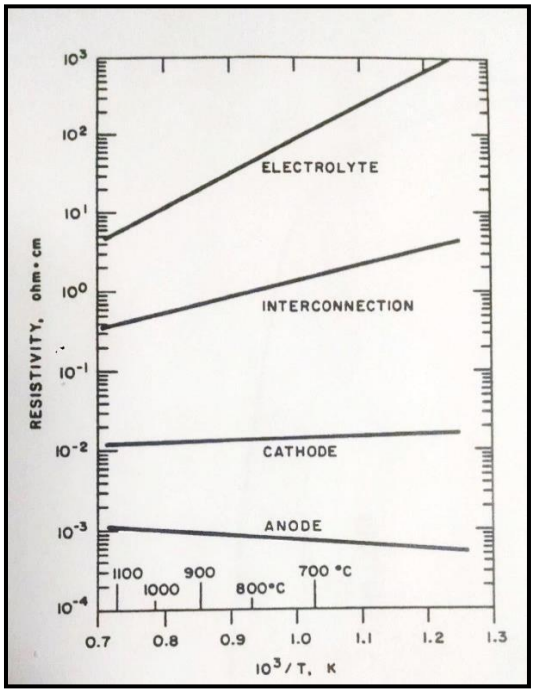


Figure 3.6: Resistivity chart (Fee, et al; 1983)

The thickness of the YSZ button cell is 0.26 mm, which was measured with a vernier caliper.

The active area of the button cell corresponds to the area of the porous electrodes, which was based on the length of the largest square that could fit into the YSZ circle as shown in Figure 3.7. The length, L, is:

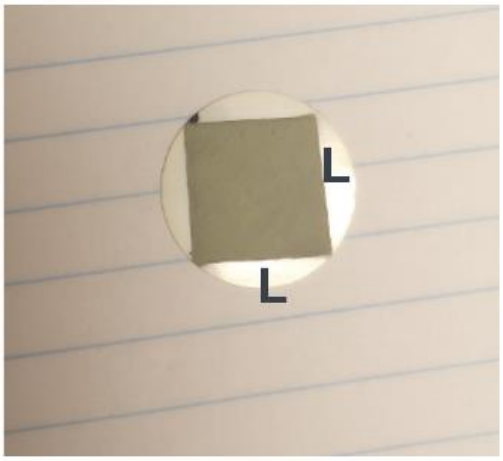


Figure 3.7: YSZ button cell showing the area of the electrode coating.

$L = r\sqrt{2}$

Hence, L = 1.414 cm

Therefore, $A$ = 2.0 $cm^2$

Recall, $R = \rho\, l/A$

R = 40 x 0.0260 / 2

R = 0.52 Ω

The button cell did not offer a high resistance to the system when compared to the slope of 11.22 Ω obtained under hydrogen in Figure 3.5. The difference between theory and the measured resistance can be attributed to the charge transfer resistance of anode and cathode under load.

## Pt/YSZ/Pt BUTTON CELL RUN ON METHANE AND AIR AT 750 °C

The button cell is purged by bubbling argon through it for about 10-15 min. This is done to purge the hydrogen from the anode of the cell before following it up with methane gas at a flow rate of 50 ml/min through the humidification vessel. The temperature of the vessel is maintained at 89 °C using a variable controller so as to maintain the pressure of the water bath at 506 torr, or 67% humidity.

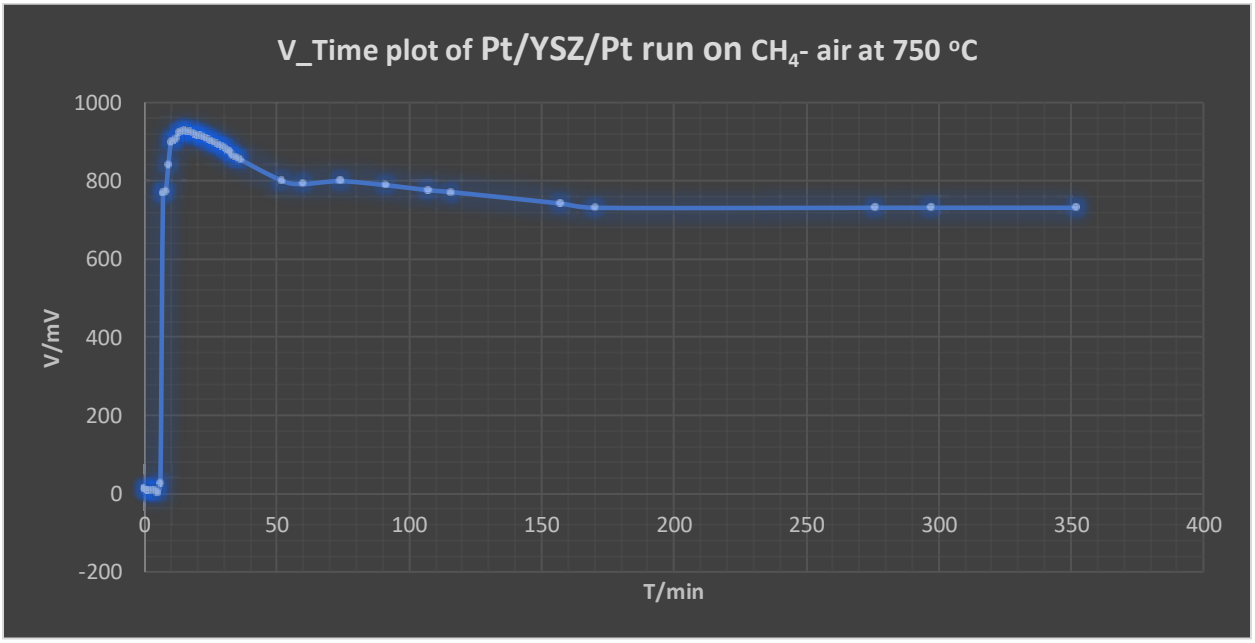


Figure 3.8: V_Time plot of the Pt/YSZ/Pt run on methane and air at 750 °C.

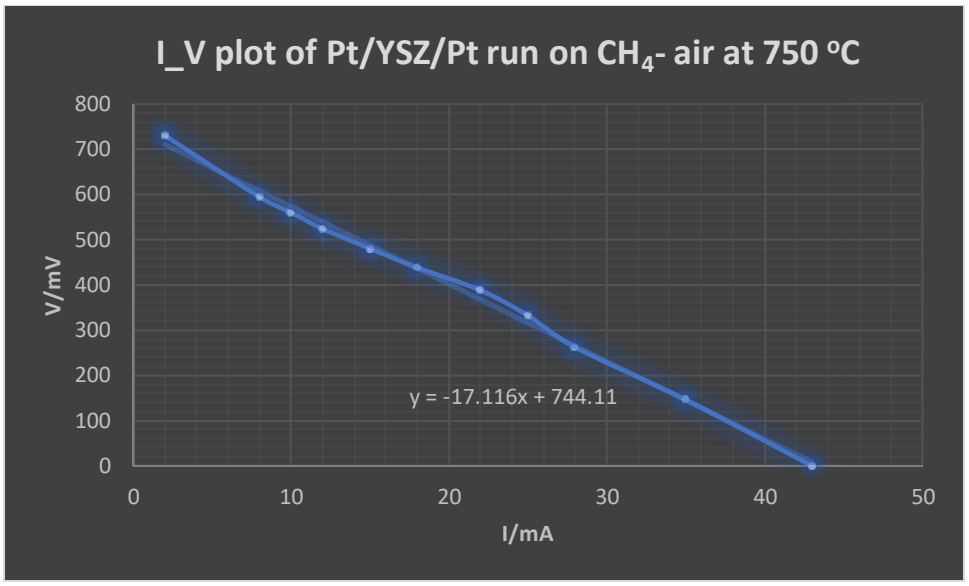


Figure 3.9: V vs I plot of the Pt/YSZ/Pt run on methane and air at 750 °C

Figures 3.8 and 3.9 shows a voltage-time and the current- voltage graph of the button cell over 350 min. It took about 6 min for the cell to respond to the methane gas, and nearly 3 h for a steady state to be attained.

There is a slight fall in voltage from a peak value of 929 mV to a steady state value of 731 mV, as seen in Figure 3.8, which was thought to be due to the carbon deposition that has accumulated on the surface of the cell's anode.

## REGENERATION TEST

To check if the cell can regain its original form, it is purged using argon to chase out the methane gas and is allowed to sit in the air for 24 hours to clean the cell from carbon that has accumulated on the surface of the cell anode as a result of the exposure to methane. After the air treatment, it is purged with argon again to chase out the air in the system before it is run on hydrogen, and the resulting voltage-current curve is shown in Figure 3.10.

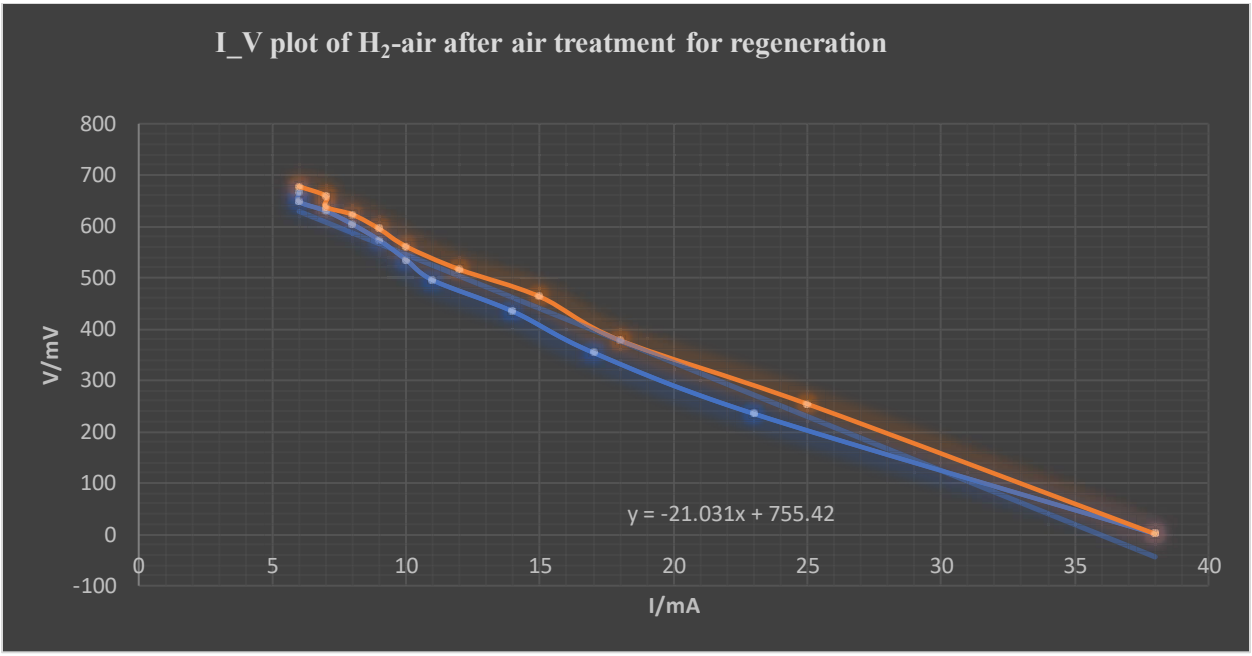


Figure 3.10: I_V plot of the Pt/YSZ/Pt run on hydrogen after air treatment for regeneration at 750 $^{o}$C.

Obtaining steady state values with a variable load imposed on the cell, the slope of the current-voltage curve, which is also the resistance of the cell, was calculated to be 21 Ω, which is double the resistance (11 Ω) obtained from a fresh button cell in Figure 3.5. This increase in the resistance of the cell is attributed to residual carbon that survived the air treatment, or could be a slight loss of electrode surface area resulting from cycling between oxidizing and reducing atmospheres.

The hydrogen is replaced with argon before following it with methane gas, and the voltage-time curve generated is shown in Figure 3.11 below.

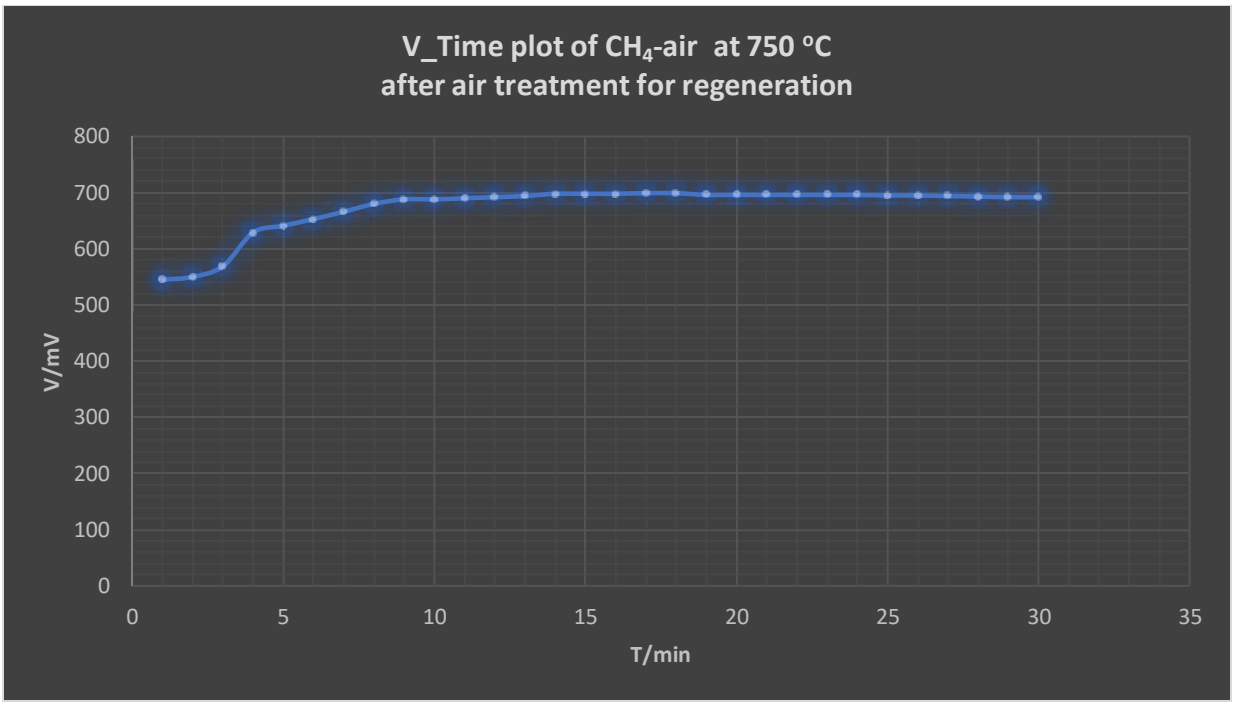


Figure 3.11: V_Time plot of the Pt/YSZ/Pt run on methane after air treatment for regeneration at 750 °C.

The graph shows a steady rise in voltage to a peak value of 692 mV. However, upon comparing this peak voltage to the peak voltage of 731 mV obtained from a fresh button cell in Figure 3.8, it is evident that the cell's performance was still below par even after air treatment. The decrease in voltage to 692 mV and the cell's failure to fully regain its initial voltage of 731 mV are attributed to the accumulation of carbon on the surface of the cell's anode, which increases the electrode polarization and results in a decrease in the voltage.

The button cell was further investigated by removing and analyzing it using a SEM/EDS instrument. The data obtained are shown in Figure 3.12 and Table 3.2.

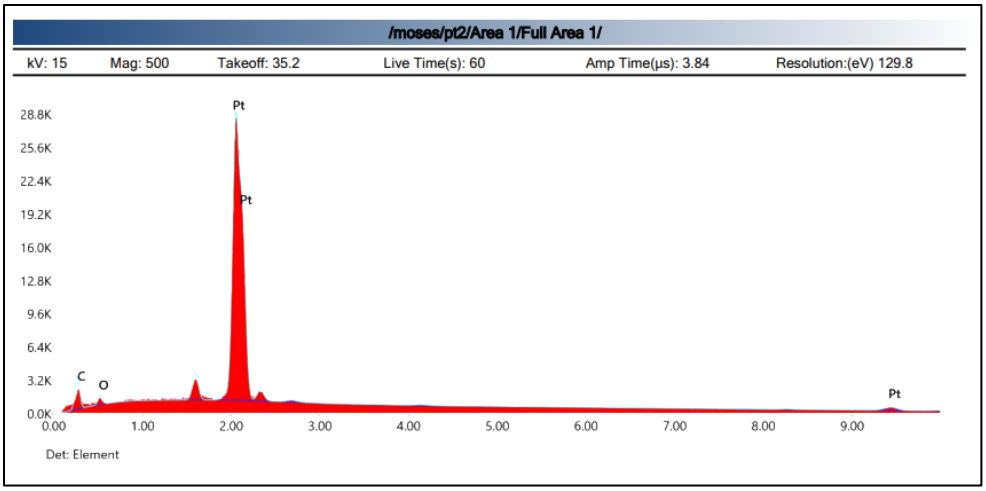


Figure 3.12: EDS graph of Pt/YSZ after air treatment and run on methane.

Table 3.2: SEM/EDS DATA OF ELEMENTAL COMPOSITION

| Element | Weight % | MDL | Atomic % | Error % |
|---|---|---|---|---|
| C K | 13.83 | 0.62 | 65.91 | 12.48 |
| O K | 2.69 | 0.24 | 9.61 | 13.6 |
| Pt M | 83.48 | 0.43 | 24.48 | 4.8 |

The data obtained from the SEM/EDS analysis indicates the presence of carbon in the sample by showing a peak in the carbon signal. The atomic percentage of carbon is 65.91, which indicates that carbon covers nearly two-thirds of the total surface area of the button cell. The black carbon soot observed on the surface of the Pt button cell and some parts of the Probostat as shown in Figure 3.13 is likely the result of incomplete combustion of methane, which appears as soot on the surface of the Pt button cell and some parts of the Probostat, leaving behind a visible black residue.

Figure 3.13: Carbon soot tainting the Pt button cell and the Probostat.

## Ni/YSZ/LSM RUN ON HYDROGEN AND AIR AT 750 $^{O}$C

The button cell mounted to the Probostat is first run on hydrogen and air as the anode and cathode gases, respectively, at a temperature of 750 $^{o}$C. The voltage-time and current-voltage curves are generated as shown in Figures 3.14 and 3.15, respectively.

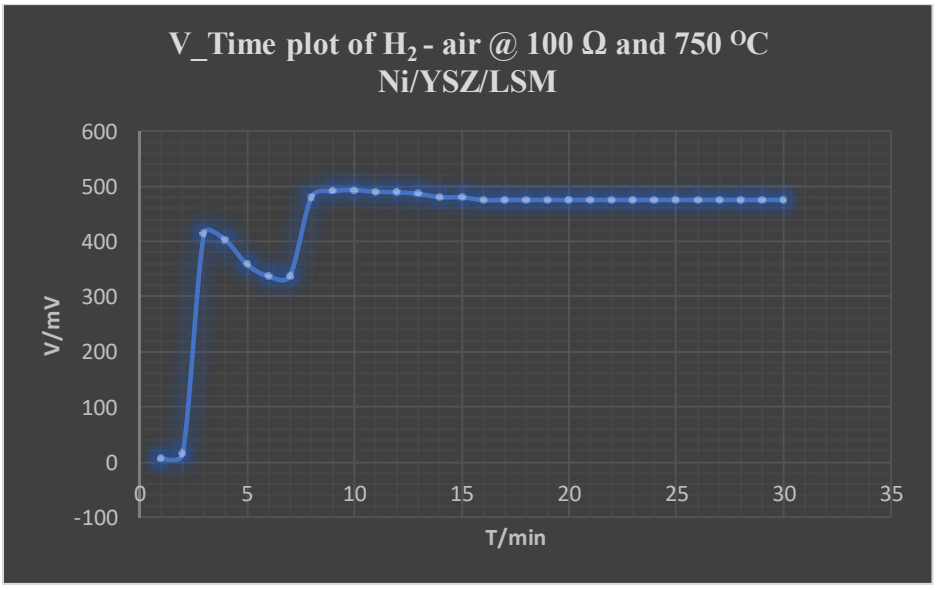


Figure 3.14: V vs Time plot of Ni/YSZ/LSM run on hydrogen and air at 750 $^{o}$C

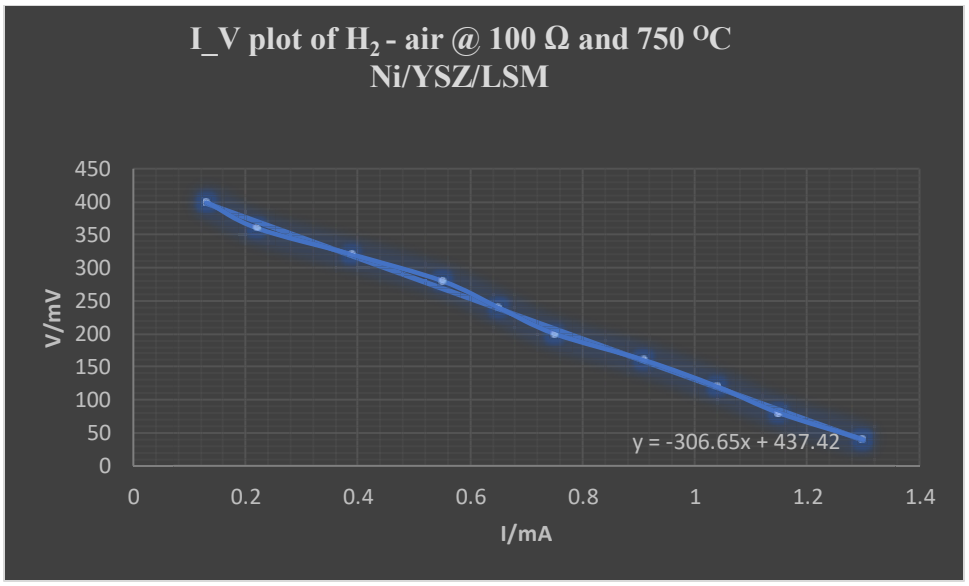


Figure 3.15: V vs I graph of Ni/YSZ/LSM run on hydrogen and air at 750 °C.

The voltage-time curve in Figure 3.14 showed a sudden increase to 400 mV in about 3 min, followed by a slight decrease to about 310 mV, which is believed to be due to an electrochemical process where nickel oxide was reduced to nickel metal, which consumes electrons. These electrons are generated during the fuel oxidation reaction at the anode and are transported through an external circuit to the cathode, where they react with oxygen to produce mobile lattice oxide ions. This reduction process may decrease the number of electrons available for the air reduction reaction at the cathode, leading to a drop in potential. However, the curve eventually stabilized and continued to rise until it reached a steady state of 490 mV after about 20 min.

Figure 3.15 displays the voltage-current relationship under a load applied to the system. The system exhibits a high resistance of 306 Ω, which may be due to electrical contact within the system. The cell attains a maximum power of 156 µW.

.

## Ni/YSZ/LSM RUN ON HUMIDIFIED METHANE AND AIR AT 750 $^{o}$C

After running the cell on hydrogen, it is purged with argon for about 10 min before following up with humidified methane gas. The voltage-time and the current-time curves, which mimic each other as well as the voltage - time curve are shown in Figures 3.16, 3.17 and 3.18, respectively. The load resistance for these curves was 100 Ω instead of 10,000 so that the currents obtained would be easily measurable.

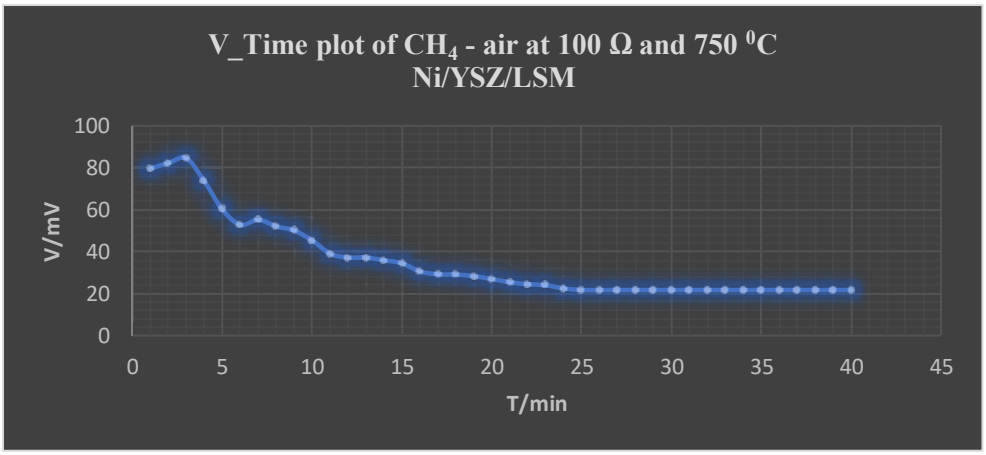


Figure 3.16: Voltage/time profile for Ni/YSZ/LSM on humidified methane gas at 750 $^{o}$C.

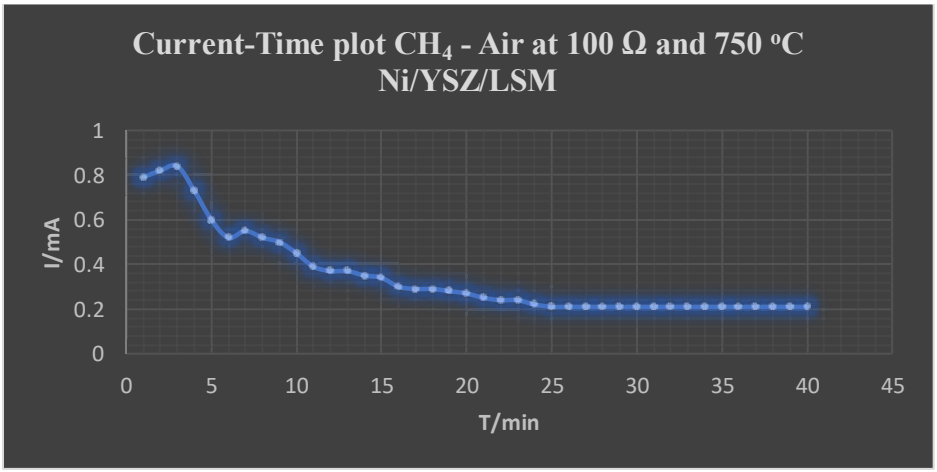


Figure 3.17: Current/time profile for Ni/YSZ/LSM on humidified methane gas at 750 $^{o}$C.

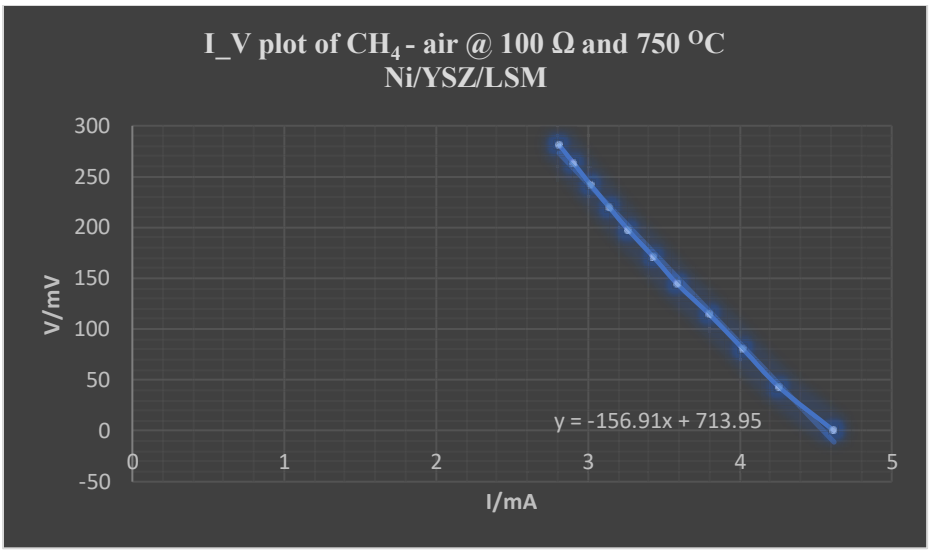


Figure 3.18: V vs I graph of Ni/YSZ/LSM run on methane and air at 750 °C.

The graphs show a steady decrease in both voltage and current values, starting from their peak values of 85 mV and 0.85 mA, respectively to reach a steady state value of 20 mV and 0.2 mA after 25 min. The maximum power produced by the cell is 156 $\mu W$.

The steady decay in the performance of the Ni/YSZ/LSM cell in humidified methane gas at 750 °C is once again due to carbon deposit formation on the surface of the cell's anode, which can lead to a decrease in the active surface area of the anode and reduce the cell's overall performance. Carbon deposit formation can occur due to the side reactions between the methane gas and the anode material, leading to the formation of carbon-rich species that can deposit on the surface of the anode and negatively impact its performance.

$$CH_4 \xrightarrow{\text{Fast}} C + 2H_2$$

However, a steady state is attained because the rate of carbon deposition on the cell's anode is balanced by its rate of removal by combining with steam and oxygen ions in the system to form carbon dioxide, as illustrated in the equations below.

$$C + H_2O \longrightarrow CO + H_2$$

$$CO + H_2O \longrightarrow CO_2 + H_2$$

$$C + 2O^{2-} \longrightarrow CO_2 + 4e^-$$

After completion of the experiment, the cell is removed and analyzed with SEM/EDS, as shown in Figure 3.19 and Table 3.3, respectively.

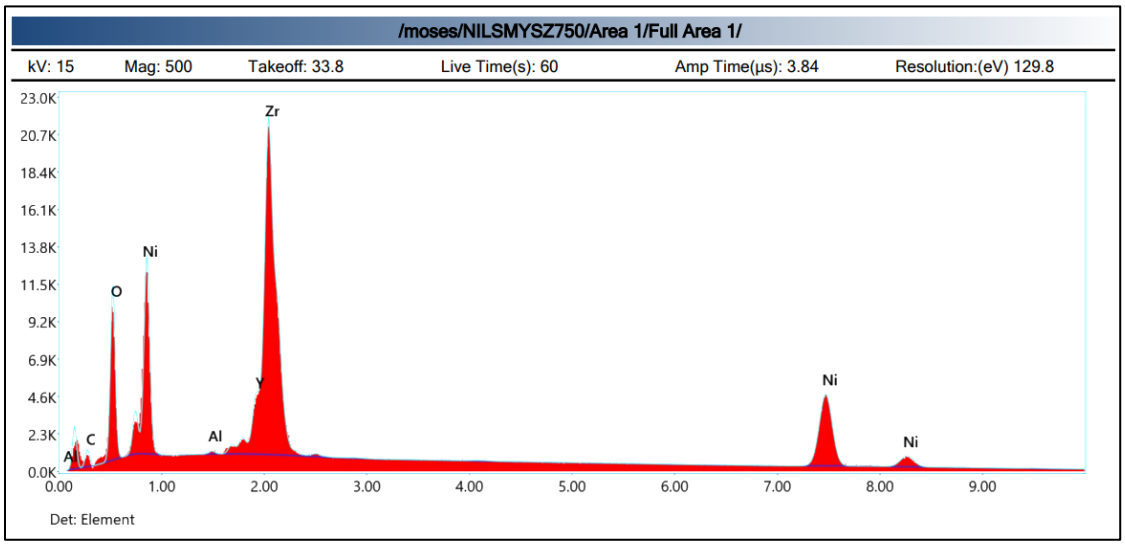


Figure 3.19: SEM/EDS of Ni/YSZ button cell at 750 °C

Table 3.3: SEM/EDS DATA OF ELEMENTAL COMPOSITION at 750 °C

| Element | Weight % | MDL | Atomic % | Error % |
|---|---|---|---|---|
| C K | 9.51 | 1.8 | 26.87 | 14.18 |
| O K | 18.52 | 0.41 | 29.26 | 10.12 |
| Al K | 0.13 | 0.18 | 0.16 | 22.87 |
| Ni K | 33.6 | 2.24 | 19.43 | 3.72 |
| Y L | 5.57 | 0.43 | 2.13 | 5.77 |
| Zr L | 32.68 | 0.45 | 12.15 | 4.59 |

The SEM/EDS graph in Figure 3.19, shows the presence of a carbon peak at ~ 27 mole percent of the total elements detected, which could certainly be responsible for the cell's poor performance under methane compared to hydrogen gas. Despite this, the cell ultimately attained a steady state.

## Ni/YSZ/LSM RUN ON METHANE AND AIR AT 800 $^{O}$C

In order to observe the effect of temperature, the experiment was repeated using a fresh Ni/YSZ/LSM substrate with the furnace temperature set at 800 $^{o}$C. The resulting data is presented in Figures 3.20 and 3.21, showing the voltage-time and current-time curves, respectively.

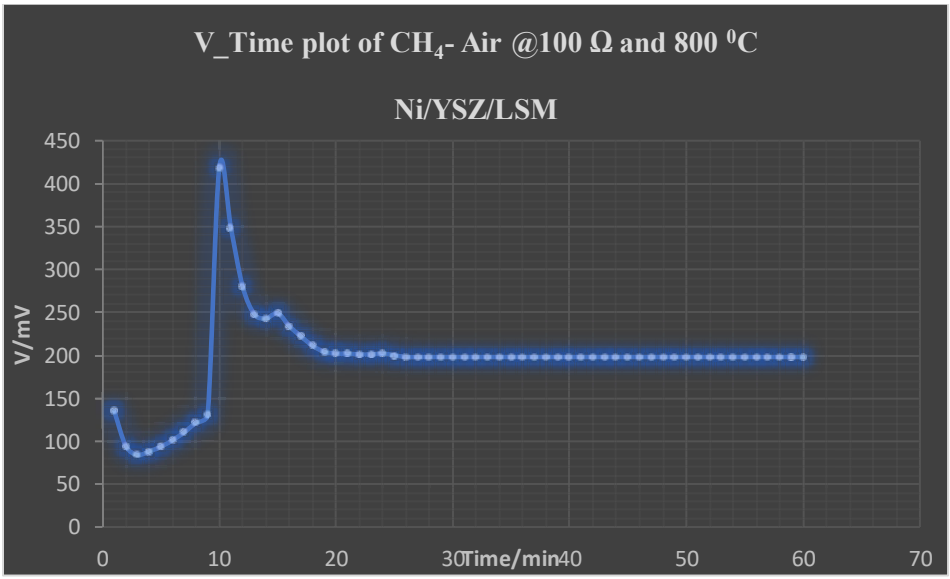


Figure 3.20: Ni/YSZ/LSM on humidified methane gas at 800 $^{O}$C.

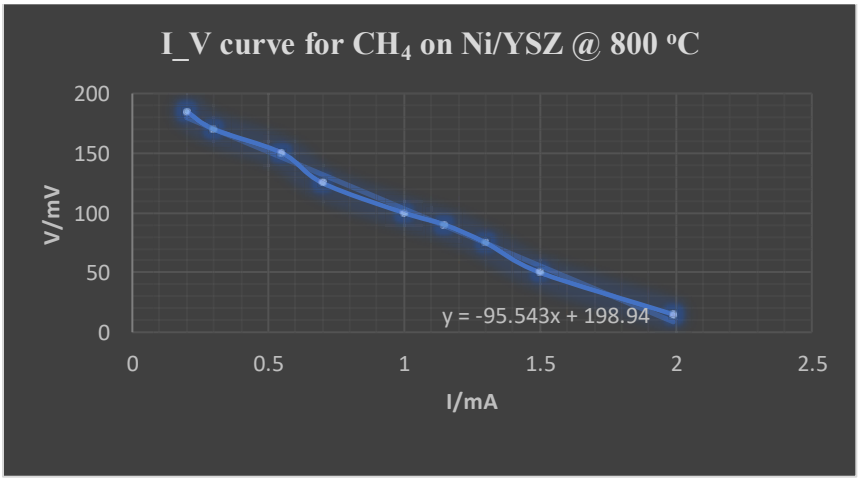


Figure 3.21: I_V of Ni/YSZ/LSM run on humidified methane and air at 800 $^{o}$C.

Figure 3.20 shows that the voltage initially rises rapidly, reaching a peak value of 430 mV within the first 10 min, before gradually declining to a steady state value of 200 mV after 20 min. Importantly, the steady-state voltage attained in this experiment is ten times higher than that achieved in the previous experiment conducted at a temperature of 750 $^{o}$C.

The plot displayed in Figure 3.21 exhibits the voltage-current relationship, which indicates the voltage and current values as a load is imposed on the system. The maximum power output generated by the cell is 103.5 $\mu$W.

The double peak seen in Figure 3.20 may be attributed to various factors. One possible cause is methane reforming, which produces CO and $H_2$. These gases are then consumed in the electrochemical reaction, resulting in a double peak voltage curve. Another possible explanation is related to the anode material's catalytic properties. Methane reforming may cause carbon deposition on the anode surface, reducing the cell's performance. The deposited carbon can also act as a catalyst for the electrochemical reaction, leading to a double peak in the voltage curve.

After completion of the experiment, the cell is removed and analyzed with SEM/EDS, as shown in Figure 3.22 and Table 3.4, respectively.

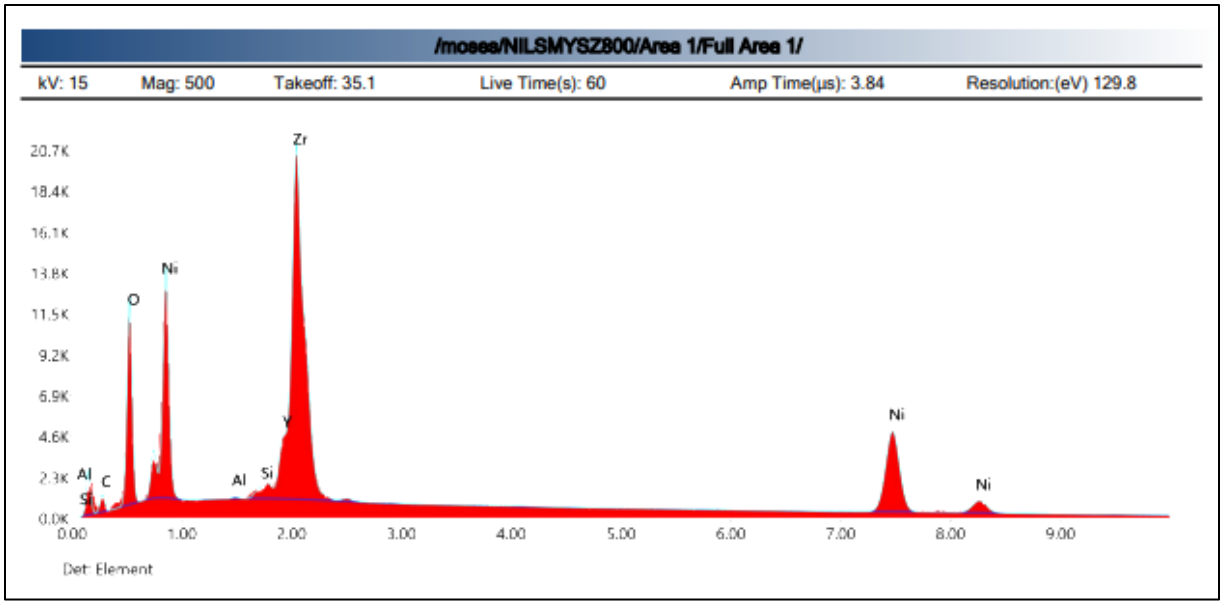


Figure 3.22: SEM/EDS of Ni/YSZ button cell operated at 800 °C.

Table 3.4: SEM/EDS DATA OF ELEMENTAL COMPOSITION AT 800 °C

| Element | Weight % | MDL | Atomic % | Error % |
|---|---|---|---|---|
| C K | 8.68 | 1.72 | 24.7 | 14.23 |
| O K | 19.07 | 0.38 | 40.71 | 10 |
| Al K | 0.06 | 0.17 | 0.08 | 51.54 |
| Si K | 0.2 | 0.16 | 0.24 | 14.32 |
| Ni K | 34.97 | 2.25 | 20.35 | 3.7 |
| Y L | 5.31 | 0.43 | 2.04 | 5.89 |
| Zr L | 31.71 | 0.45 | 11.87 | 4.58 |

The SEM/EDS graph in Figure 3.22 shows the presence of a carbon peak with a 24.7 mole percent, which could be responsible for the cell's poor performance under methane compared to hydrogen gas. Despite this, the cell ultimately attained a steady state.

## Ni/YSZ/LSM RUN ON METHANE AND AIR AT 850 $^{O}$C

The experiment was repeated using a fresh Ni/YSZ/LSM substrate, and the furnace temperature was set at 850 $^{o}$C. The experiment results are shown in Figures 3.23 and 3.24, which show the voltage-time and current-time curves, respectively.

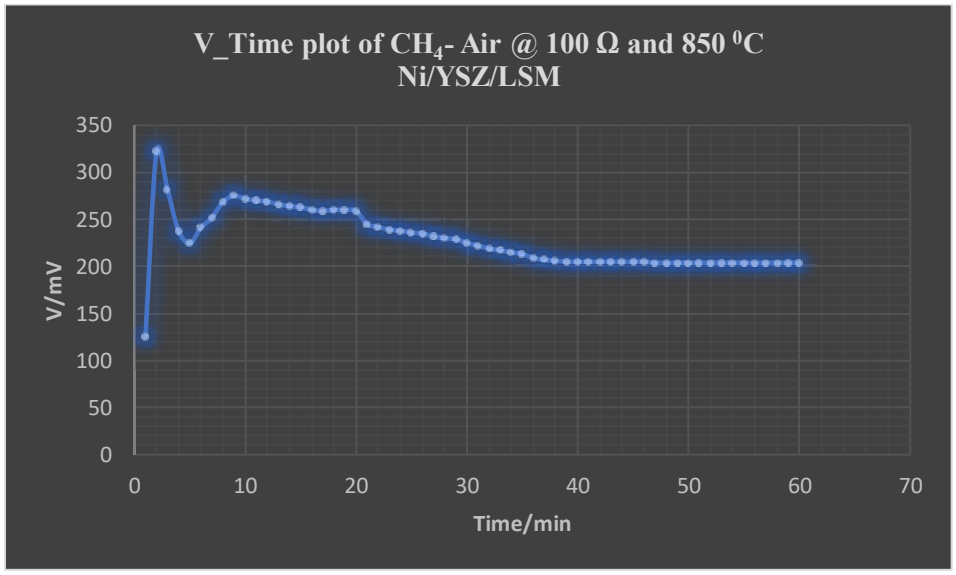


Figure 3.23: Ni/YSZ/LSM in humidified methane gas at 850 $^{o}$C.

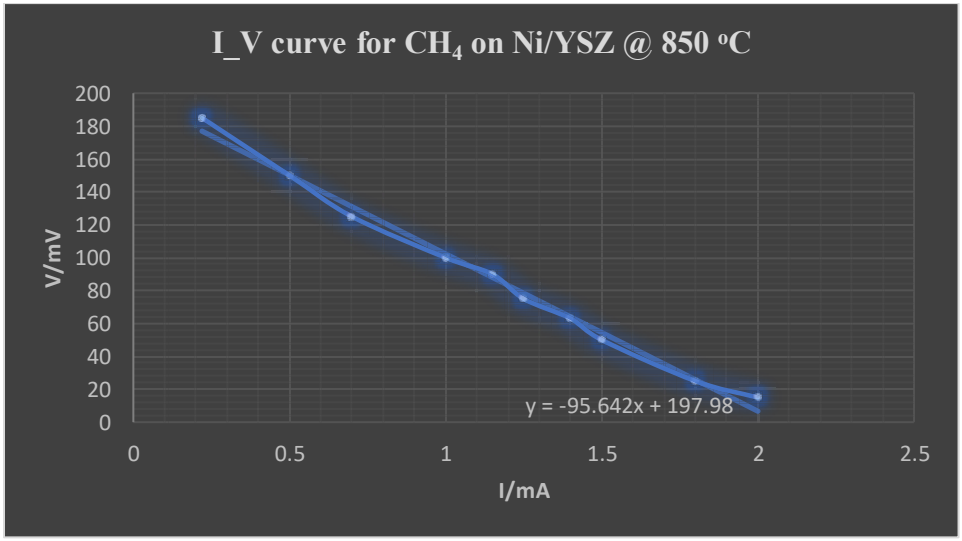


Figure 3.24: V vs I for Ni/YSZ/LSM run on humidified methane and air at 850 $^{o}$C.

Figure 3.23 displays the voltage-time curve of the cell, which shows that the voltage rapidly increases to a peak value of 330 mV before gradually decreasing to a steady-state value of 200 mV. This steady-state voltage is the same as that observed in the previous experiment conducted at 800 $^{o}$C. It is also ten times higher than the voltage achieved in the previous experiment at a temperature of 750 $^{o}$C.

The voltage-current relationship is depicted in Figure 3.24, illustrating the voltage and current values under a load applied to the system. The steady-state values closely match the curve obtained at 800 oC, as evidenced by the slope that corresponds to the cell's resistance.

The double peak phenomenon observed in the previous experiment conducted at 800 $^{o}$C is also observed in this experiment conducted at 850 $^{o}$C.

After completion of the experiment, the cell is removed and analyzed with SEM/EDS, as shown in Figure 3.25 and Table 3.5, respectively.

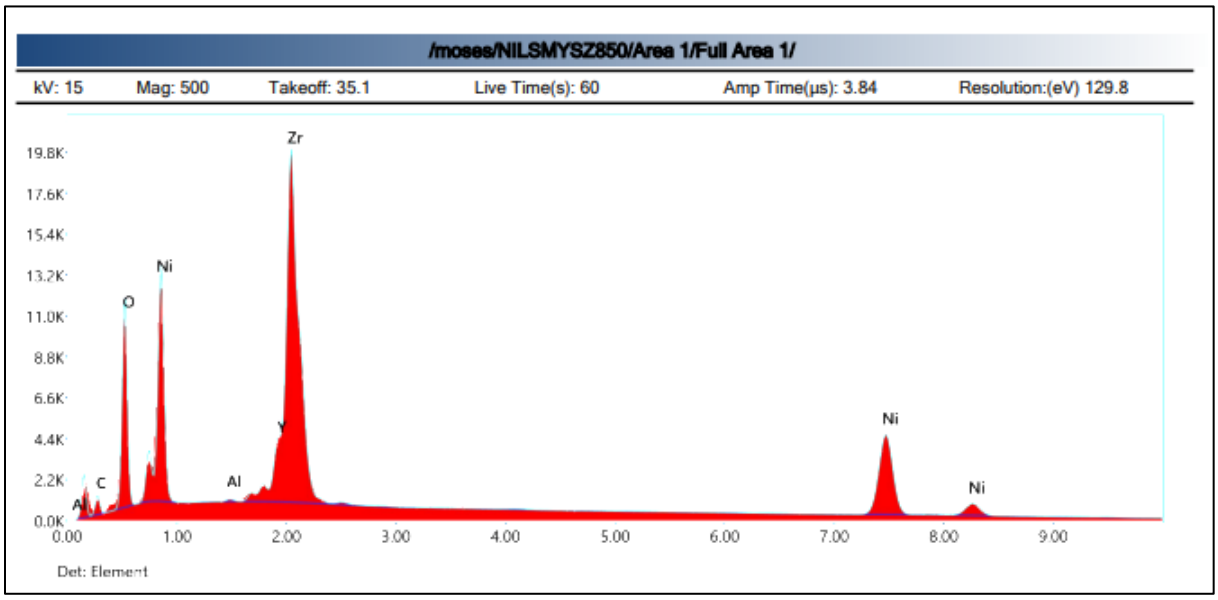


Figure 3.25: SEM/EDS graph of Ni/YSZ button cell at operated 850 $^{o}$C

Table 3.5 SEM/EDS DATA OF ELEMENTAL COMPOSITION AT 850 °C

| Element | Weight % | MDL | Atomic % | Error % |
|---|---|---|---|---|
| C K | 9.23 | 1.78 | 25.89 | 14.12 |
| O K | 19.23 | 0.4 | 40.48 | 10.01 |
| Al K | 0.1 | 0.18 | 0.12 | 30.07 |
| Ni K | 34.62 | 2.37 | 19.87 | 3.71 |
| Y L | 5.36 | 0.45 | 2.03 | 5.82 |
| Zr L | 31.46 | 0.47 | 11.62 | 4.58 |

Figure 3.25 is an SEM/EDS graph indicating the presence of a carbon peak with an atomic abundance of 25.89 mole percent, which accounts for the poor performance of the cell when run on methane gas as compared to hydrogen gas. However, it is important to note that the cell eventually reached a stable state.

## Ni/YSZ/LSM RUN ON METHANE AND AIR AT 900 $^{O}$C

The experiment was repeated using a fresh Ni/YSZ/LSM substrate, and the furnace temperature was set at 900 $^{o}$C. The experimental results are shown in Figures 3.26 and 3.27, which show the voltage-time and current-voltage curves, respectively.

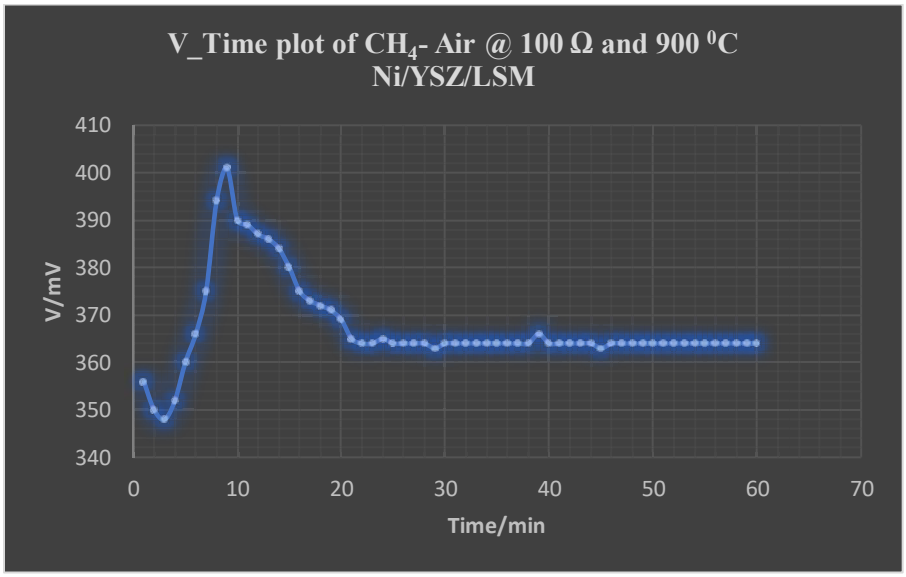


Figure 3.26: V vs Time for Ni/YSZ/LSM in humidified methane gas at 900 $^{o}$C.

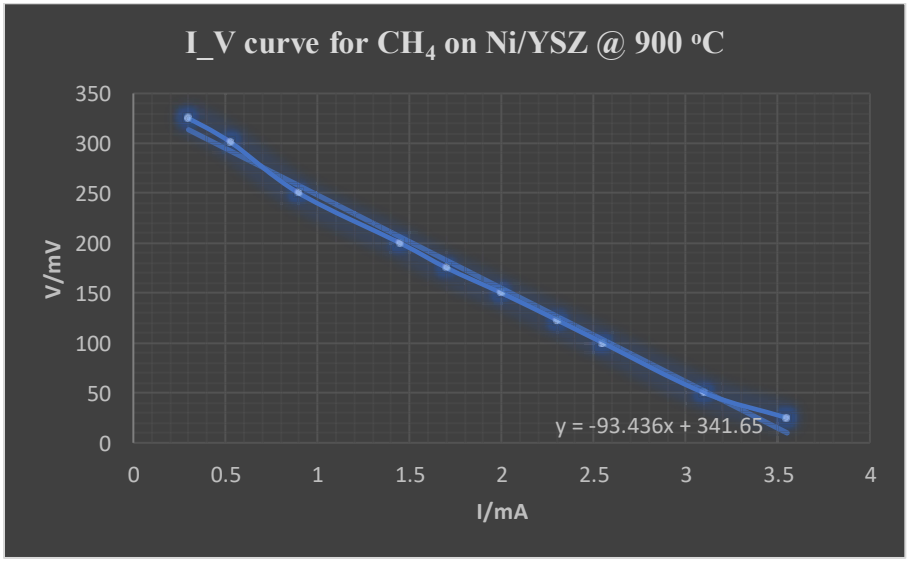


Figure 3.27: V vs I for Ni/YSZ/LSM run on humidified methane and air at 900 $^{o}$C.

Figure 3.26 displays the voltage-time curve of the cell, which shows that the voltage rapidly increases to a peak value of 402 mV before gradually decreasing to a steady-state value of 362 mV. This is significantly larger than what was measured at lower temperatures.

Figure 3.27 is the current - voltage curve with a resistance of 94 Ω. The maximum power produced by the curve is 300 $\mu W$ at a resistance of 50 Ω.

The double peak phenomenon observed in the previous experiment conducted at 800 °C and 850 °C is also observed in this experiment conducted at 900 °C.

After completion of the experiment, the cell is removed and analyzed with SEM/EDS, as shown in Figure 3.28 and Table 3.6, respectively.

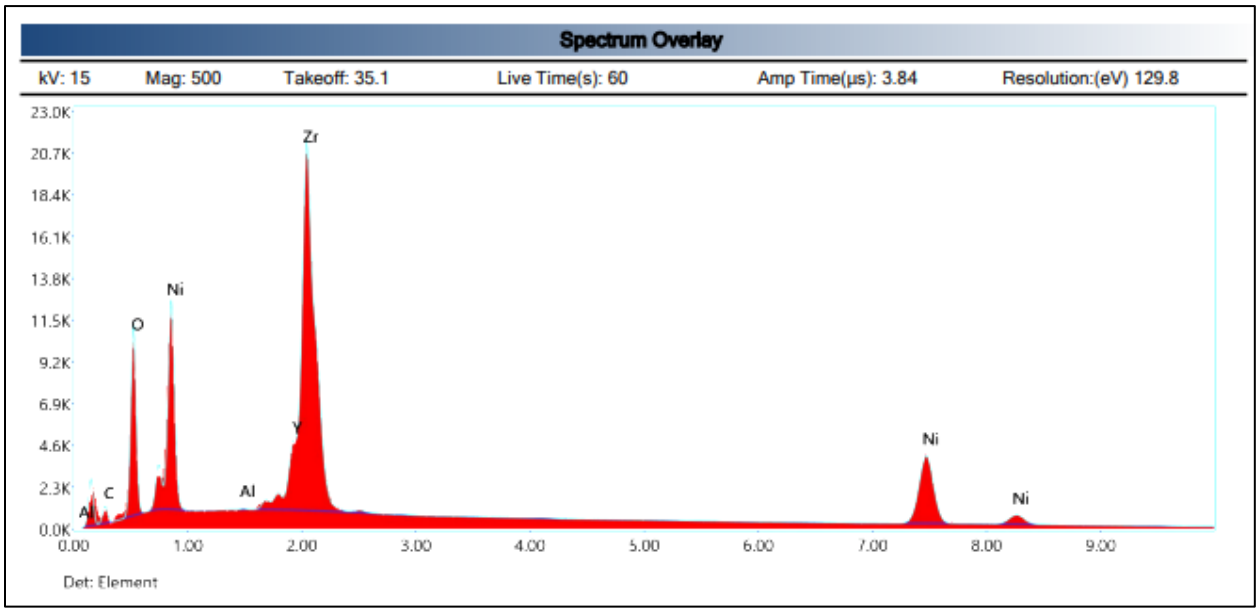


Figure 3.28: SEM/EDS of Ni/YSZ button cell run on humidified methane at 900 °C.

Table 3.6: SEM/EDS DATA OF ELEMENTAL COMPOSITION AT 900 $^{0}$C

| Element | Weight % | MDL | Atomic % | Error % |
|---|---|---|---|---|
| C $_{K}$ | 9.31 | 1.9 | 26.13 | 14.3 |
| O $_{K}$ | 19.53 | 0.44 | 41.15 | 10.09 |
| Al $_{K}$ | 0.04 | 0.17 | 0.05 | 66.19 |
| Ni $_{K}$ | 30.87 | 2.44 | 17.74 | 3.8 |
| Y $_{L}$ | 5.95 | 0.46 | 2.26 | 5.58 |
| Zr $_{L}$ | 34.31 | 0.48 | 12.08 | 4.49 |

Figure 3.28 shows a SEM/EDS graph that illustrates the presence of a carbon peak at a level of 26.13 mole percent, which could potentially explain why the cell had poor performance when run on methane in contrast to hydrogen gas. Despite this, the cell ultimately attained a steady state.

## EXPERIMENT WITH MAHONING LANDFILL GAS

The Mahoning Landfill in New Springfield, Ohio, is a green project that uses its biogas arising from bacterial digestion of municipal solid waste as a source of renewable energy. The landfill gas is a combination of various gases, with methane being the most abundant, making it a valuable energy source.

To capture LFG, the Mahoning Landfill Gas project employs a network of wells and pipes, which then undergoes a purification process to remove impurities like moisture, sulfur compounds, and volatile organic compounds. After purification, the LFG is utilized as a fuel source to generate electricity that is sold to the power grid.

The Mahoning Landfill Gas Project has a 4.8-megawatt capacity, sufficient to power approximately 4,000 households. (*https://vindyarchives.com/news/2013/feb/25/trash-to-treasure)*

Figure 3.29: Wellhead for landfill gas at the Mahoning Landfill.

About 60 liters of mildly pressurized (35 psi) landfill gas was collected and brought to the laboratory to apply to the button cell.

Figure 3.30: Pressurized gas cylinders containing landfill gas.

The pressurized landfill gas is connected to a flow meter set to 50 ml/min and goes through a sulfur scrubber to remove any traces of sulfur before being channeled to a humidifying vessel. In the humidifying vessel, the siloxanes in the gas are intermingled with water vapor, causing them to break down into silica particles before the gas gets to the anode of the button cell. The air is delivered to the cathode of the cell from the air cylinder. Figure 3.30 below shows the process flow diagram.

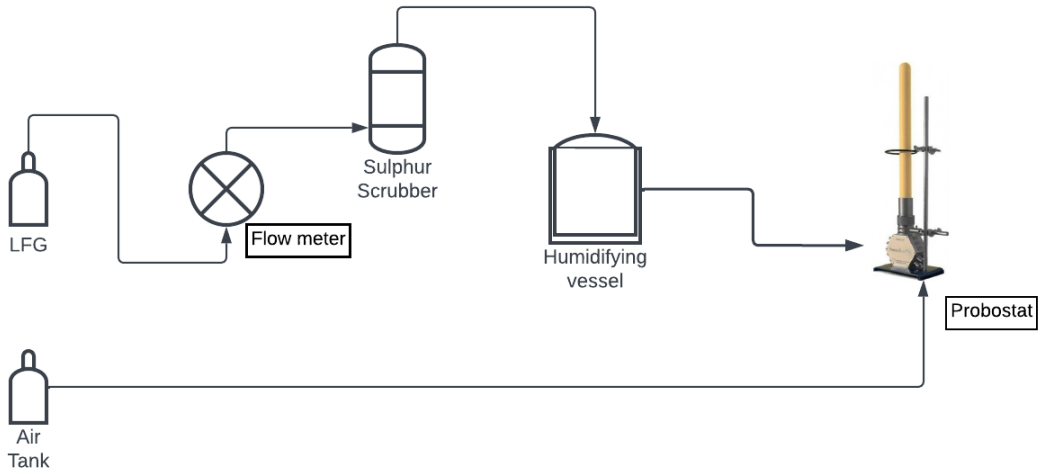


Figure 3.31: Flow diagram for the landfill gas operation.

## EXPERIMENTAL RESULTS WITH MAHONING LANDFILL GAS

The reduced button cell, after running on hydrogen at 800 °C, was purged with argon gas to remove the hydrogen before introducing the landfill gas. With a resistance of 9999 Ω imposed on the system, the voltage-time curve of the cell decreased gradually from 833 mV to 642 mV after about 30 min to reach a steady state as shown in Figure 3.32.

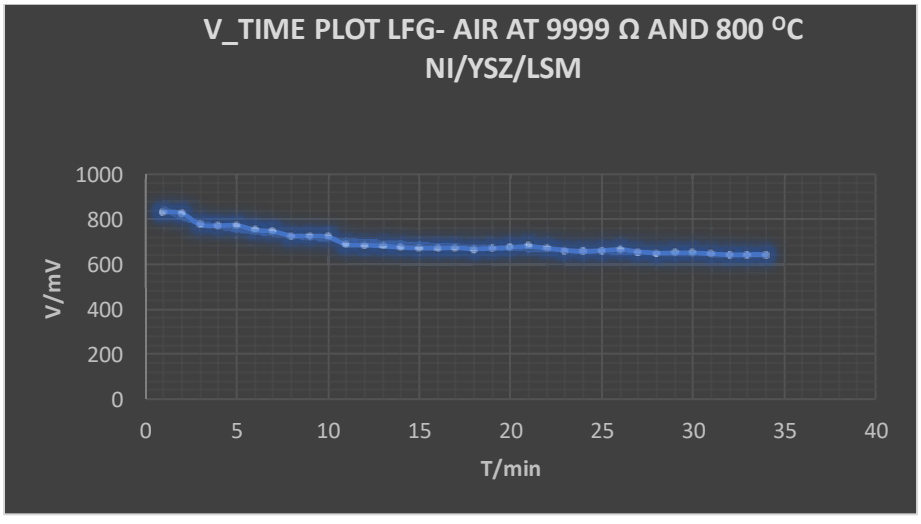


Figure 3.32: V vs Time for Ni/YSZ/LSM run on landfill gas at 800 °C.

After achieving the steady state, the resistor box was dialed down from 9999 Ω to 20 Ω to obtain a corresponding voltage-current plot for the assembly.

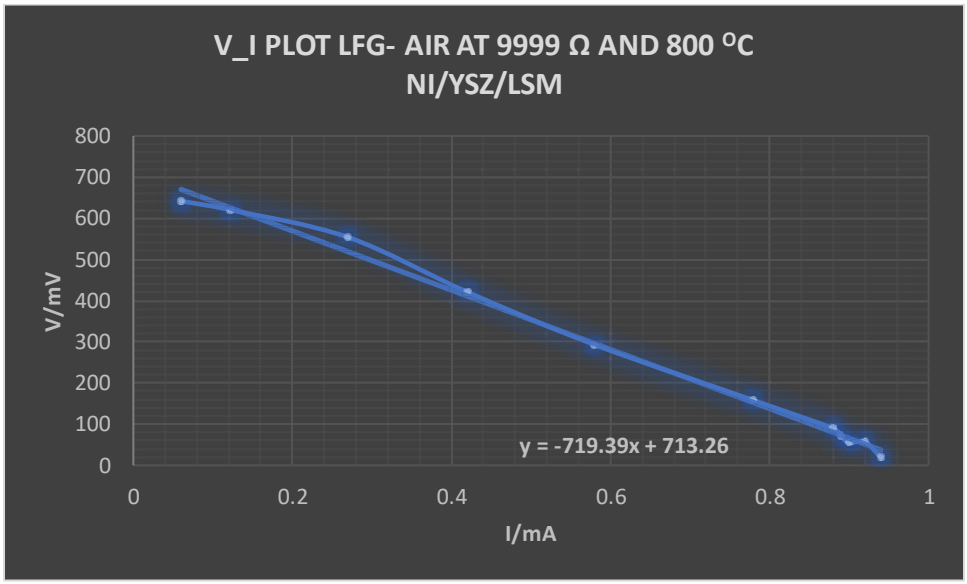


Figure 3.33: V vs I plot for Ni/YSZ/LSM run on landfill gas at 800 °C.

The high resistance of 719 Ω observed in the cell could be attributed to contact problems or contaminants within the cell, which explains the low current generated by the cell, which was 0.94 mA at 20 Ω load resistance.

## EXPERIMENTAL RESULTS WITH SIMULATED LANDFILL GAS

In order to make a better comparison with the results obtained with the real landfill gas, a Ni/YSZ/LSM button cell was run on a simulated landfill gas blend of 10 parts of $CH_4$ (25 ml/min), 7 parts of $CO_2$ (17.5 ml/min), and 3 parts $N_2$ (7.5 ml/min) to make up a total flow rate of 50 ml/min, not including the two-thirds water vapor content, as these are the major constituents of landfill gas. The voltage-time graph and the current-voltage plot obtained are shown in Figures 3.34 and 3.35 below.

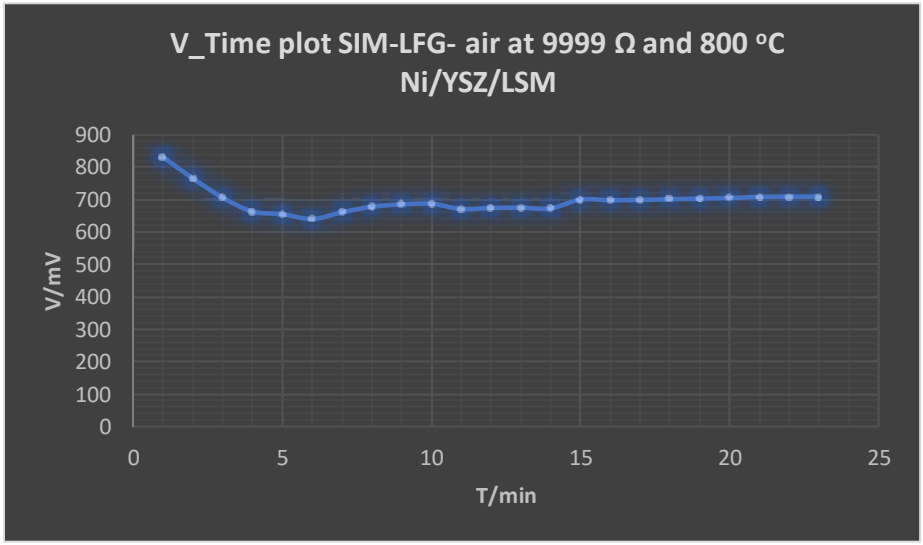


Figure 3.34:V vs Time plot for Ni/YSZ/LSM run on simulated landfill gas at 800°C.

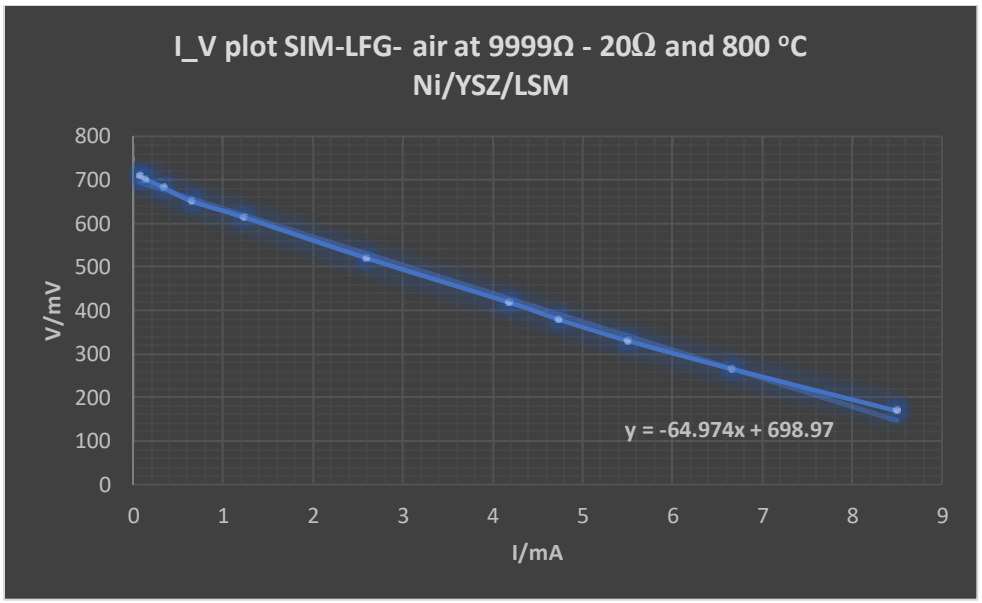


Figure 3.35: V vs I plot for Ni/YSZ/LSM run on simulated landfill gas at 800 °C.

The voltage of the cell drops steadily from 800 mV until it levels out to a steady state after about 22 min. The current-voltage time plot shows the cell resistance was down to 65 Ω, which indicates good connectivity and contact within the cell. The maximum current drawn by the button cell was 8.5 mA.

The current-voltage curves for the real landfill gas and the simulated landfill gas as shown together in Figure 3.36, the two curves did not overlap because the charge transfer resistance for landfill gas was decidedly higher. The maximum power for the simulated LFG was 1818 $\mu$W compared to the maximum power for the real LFG, which was 176.82 $\mu$W, a 90% drop.

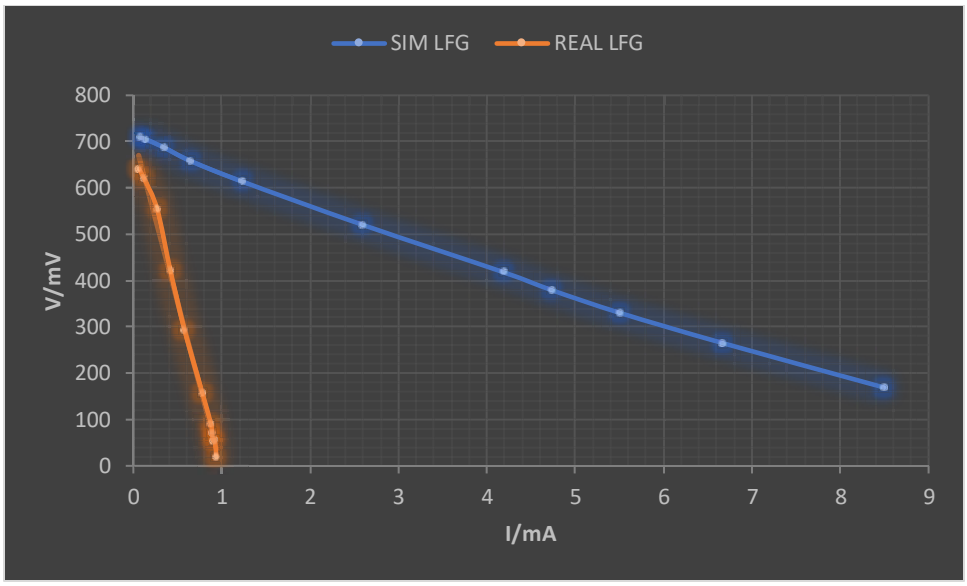


Figure 3.36: V vs I plot for Ni/YSZ/LSM run on simulated and real landfill gas.

To determine why the button cell performed poorly when run on real landfill gas compared to simulated landfill gas, an SEM/EDS analysis was conducted on the button cell run on real landfill gas. The purpose of this analysis was to identify any contaminants that might have contributed to the cell's poor performance.

Figure 3.37 and Table 3.7 is the SEM/EDS data of the button cell run on landfill gas.

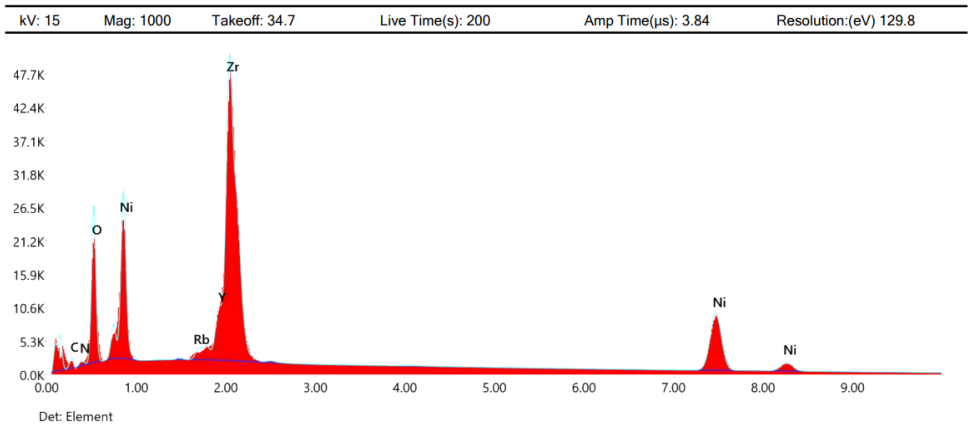


Figure 3.37: SEM/EDS graph of Ni/YSZ button cell run on landfill gas at 800 °C

Table 3.7: SEM/EDS DATA for Ni/YSZ button cell run on landfill gas at 800 °C.

| Element | Weight % | MDL | Atomic % | Error % |
|---|---|---|---|---|
| $C_K$ | 7.17 | 0.87 | 20.54 | 13.75 |
| $N_K$ | 1.64 | 0.38 | 4.02 | 15.94 |
| $O_K$ | 19.49 | 0.19 | 41.9 | 9.98 |
| $Ni_K$ | 30.76 | 1.03 | 18.03 | 3.54 |
| $Rb_k$ | 0.78 | 0.18 | 0.32 | 9.67 |
| $Y_L$ | 5.71 | 0.2 | 2.21 | 5.51 |
| $Zr_L$ | 34.44 | 0.2 | 12.99 | 4.4 |

The SEM/EDS analysis showed no indication of any harmful heavy metals present as contaminants; only carbon appeared on the anode of the cell after electrolysis.

# CHAPTER FOUR

# CONCLUSION

Carbon deposition in SOFCs can significantly impact their performance. This occurs when hydrocarbon fuels such as methane are used as the fuel source, and the carbon in the fuel accumulates on the surface of the anode, reducing its activity and conductivity.

The effects of carbon deposition on SOFC performance depend on the amount and location of the deposition. If the deposition is extensive, it can lead to reduced fuel cell efficiency, power output, and even complete failure of the cell. However, if the carbon deposition is limited and occurs in a controlled manner, it is possible for the cell to reach steady-state operation.

The SEM/EDS plots at different temperatures show a peak for carbon deposition and the percentage weight composition of the carbon on the anode of the cell.

A mole percent of 25-26 % for the extent of carbon deposition is approximately the same irrespective of the temperature from 750-900 $^{o}$C. Cell resistance, as determined by the slope of the respective voltage - current curves, is likewise nearly constant at 95 Ω. However, steady state voltage under load rose significantly over that range, suggesting an activation limited process. Overall, it can be concluded that carbon deposition affects the performance of the cell, but a steady state is nevertheless achieved.

Also, the performance of the SOFC is strongly dependent on temperature, and increasing the temperature can lead to higher steady-state voltage and current output.

At higher temperatures, the ionic conductivity of the electrolyte increases, which enhances the transport of oxygen ions through the electrolyte to the fuel electrode. Activation-limited charge transfer is also enhanced. This results in increased electrochemical activity and higher current

density at the electrode/electrolyte interface. Additionally, higher temperatures can improve the kinetics of the electrochemical reactions that occur at the electrodes, leading to a higher voltage output.

The real landfill and simulated landfill gas gave the same voltage time transients, but the current-voltage graph for the real landfill gas fell below the value obtained for the simulated landfill gas, which indicates the possibility of contamination from other agents in the landfill gas that cause the current to fall.

SEM/EDS analysis showed the presence of rubidium in trace amounts. It is not yet confirmed if this is a contributing contaminant slowing down the cell's performance. However, there could be other contaminants if a more sensitive instrument can be used to analyze the anode of the cell run on real landfill gas.

# FUTURE DIRECTIONS

Although a steady state can be achieved by operating a solid oxide fuel cell (SOFC) on landfill gas that has been purged of sulfur and siloxanes, it is essential to use more surface-sensitive instruments like XPS to examine the anode of the cell for any trace contaminants that may be impacting its performance. This will be a good next step for determining the other elements that could be impeding the performance of the cell run on landfill gas.

# REFERENCES


Afroze, S., Reza, M. S., Cheok, Q., Taweekun, J., & Azad, A. K. (2020). Solid oxide fuel cell (SOFC); A new approach of energy generation during the pandemic COVID-19. *International Journal of Integrated Engineering*, *12*(5), 245–256. https://doi.org/10.30880/ijie.2020.12.05.030

Ahmed, S. I., Johari, A., Hashim, H., Mat, R., Lim, J. S., Ngadi, N., & Ali, A. (2015). Optimal landfill gas utilization for renewable energy production. Environmental Progress & Sustainable Energy, 34(1), 289-296.

Baguer, Neyda. Numerical Modeling of a Hollow Cathode Discharge. Universiteit Antwerpen, Faculteit Wetenschappen, Departement Scheikunde, 2005.

Baldi, F., Wang, L., Pérez-Fortes, M., & Maréchal, F. (2019). A cogeneration system based on solid oxide and proton exchange membrane fuel cells with hybrid storage for off-grid applications. *Frontiers in Energy Research*, *6*(139), 1–18. https://doi.org/10.3389/fenrg.2018.00139.

Bartram, F. (2020, November 30). *Benefits of recycling*. A Good Company. Retrieved March 31, 2022, from https://agood.com/blogs/stories/benefits-of-recycling

Brinkienė, & Čėsnienė. (2008, June). Investigation of Plasma Coatings Manufactured from Synthesized Zirconia. MATERIALS SCIENCE (MEDŽIAGOTYRA)., Vol. 14, No. 2. 2008(ISSN 1392–1320), 138–142. https://www.researchgate.net/publication/228497545

Brodny, J., & Tutak, M. (2020). Analyzing similarities between the European Union countries in terms of the structure and volume of energy production from renewable energy sources. Energies, 13(4), 913.

Brostrøm, Anders, et al. "Analysis of Electron Transparent Beam-Sensitive Samples Using Scanning Electron Microscopy Coupled with Energy-Dispersive X-Ray Spectroscopy." Microscopy and Microanalysis, vol. 26, no. 3, 2020, pp. 373–386., https://doi.org/10.1017/s1431927620001464.

Dudin, M. N., Frolova, E. E., Protopopova, O. V., Mamedov, A. A., & Odintsov, S. V. (2019). Study of innovative technologies in the energy industry: Nontraditional and renewable energy sources. *Entrepreneurship and Sustainability Issues*, *6*(4), 1704–1713. https://doi.org/10.9770/jesi.2019.6.4(11)

Elavarasan, R. M. (2019). The Motivation for Renewable Energy and its Comparison with Other Energy Sources: A Review. *European Journal of Sustainable Development Research*, *3*(1), 1–19. https://doi.org/10.20897/ejosdr/4005

Environmental Protection Agency. (n.d.). EPA. Retrieved April 6, 2022, from https://www.epa.gov/lmop/basic-information-about-landfill-gas

Fee, et, al; "Solid Oxide Fuel Cell Performance," Proceedings of the Conference on High Temperature Solid Oxide Electrolytes Aug 16-17, 1983: Volume I – Anion Conductors; BNL-51728; Brookhaven National Laboratory: Upton, NY, 1983.

Gamez, M. R., Perez, A. V., Sera, A. S., & Ronquillo, Z. M. (2017). Renewable Energy Sources and Local Development. *International Journal of Social Sciences and Local Development*, *1*(2), 10–19.

Hao, X., Yang, H., & Zhang, G. (2008). Trigeneration: A new way for landfill gas utilization and its feasibility in Hong Kong. Energy Policy, 36(10), 3662–3673. https://doi.org/10.1016/j.enpol.2008.05.031

History.com Editors. (2010, August 30). *Energy crisis (1970s)*. History.com. Retrieved April 7, 2022, from https://www.history.com/topics/1970s/energy-crisis

Khan, F. (2012). *Effect of Hydrogen Sulfide in Landfill Gas on Anode Poisoning of Solid Oxide Fuel Cells* (Doctoral dissertation, Youngstown State University).

*Land of Waste: American Landfills and Waste Production*. (n.d.). Retrieved March 31, 2022, (Save on Energy, LLC), from https://www.saveonenergy.com/land-of-waste/

Laosiripojana, N., Wiyaratn, W., Kiatkittipong, W., Arpornwichanop, A., Soottitantawat, A., & Assabumrungrat, S. (2009). Reviews on solid oxide fuel cell technology. Engineering Journal, 13(1), 65-84. https://doi.org/10.4186/ej.2009.13.1.65

Measurlabs. "SEM-EDX Analysis: Laboratory Services." Measurlabs, https://measurlabs.com/methods/scanning-electron-microscopy-x-ray-spectroscopy-sem-edx/.

Norecs. (n.d.). Complementary Material to ProboStat™ Manual. Index of files. Retrieved April 14, 2023, from https://www.norecs.com/work/_files/__PUBLIC_FILES__/manuals

Ormerod, R. M. (2003). Solid oxide fuel cells. *Chemical Society Reviews*, *32*(1), 17–28. https://doi.org/10.1039/b105764m

Owusu, P. A., & Asumadu-Sarkodie, S. (2016). A review of renewable energy sources, sustainability issues and climate change mitigation. *Cogent Engineering*, *3*(1), 1167990. https://doi.org/10.1080/23311916.2016.1167990

*Probostat Versatile high temperature test fixture*. Maranata-Madrid SL - NIF B-85746204. (n.d.). Retrieved April 6, 2022, from https://www.alphaomega-electronics.com/en/norecs/2256-probostat-accesorio-de-prueba-versatil-de-alta-temperatura.html

"ProboStat™." *NORECS*, http://www.norecs.com/.

Qazi, A., Hussain, F., Rahim, N. A. B. D., Hardaker, G., Alghazzawi, D., Shaban, K., & Haruna, K. (2019). Towards Sustainable Energy: A Systematic Review of Renewable Energy

Sammer, Claudia. Alberta's Nanotechnology and Advanced Materials: Special Report. Cool Companies, 2008.

Sources, Technologies, and Public Opinions. *IEEE Access*, *7*(2019), 63837–63851. https://doi.org/10.1109/ACCESS.2019.2906402

Shahzad, U. (2012). The need for renewable energy sources. energy, 2, 16-18.

WASTE MANAGEMENT | SPECIAL TO THE VINDICATOR. “Mahoning Landfill Gas Generates Electricity, Rather than Being Wasted.” Http://Vindyarchives.com, https://vindyarchives.com/news/2013/feb/25/trash-to-treasure/.

Zivak, M. (2020). *Studying the Effects of Siloxanes on Solid Oxide Fuel Cell Performance*. Youngstown State University.